SeaWiFS Postlaunch Technical Report Series

Stanford B. Hooker and Elaine R. Firestone, Editors

Volume 19, Coastal Atmosphere and Sea Time Series (CoASTS), Part 1: A Tower-Based, Long-Term Measurement Program

Giuseppe Zibordi, Jean-Françoise Berthon, John P. Doyle, Stefania Grossi, Dirk van der Linde, Cristina Targa and Luigi Alberotanza

The NASA STI Program Office ... in Profile

Since its founding, NASA has been dedicated to the advancement of aeronautics and space science. The NASA Scientific and Technical Information (STI) Program Office plays a key part in helping NASA maintain this important role.

The NASA STI Program Office is operated by Langley Research Center, the lead center for NASA's scientific and technical information. The NASA STI Program Office provides access to the NASA STI Database, the largest collection of aeronautical and space science STI in the world. The Program Office is also NASA's institutional mechanism for disseminating the results of its research and development activities. These results are published by NASA in the NASA STI Report Series, which includes the following report types:

- TECHNICAL PUBLICATION. Reports of completed research or a major significant phase of research that present the results of NASA programs and include extensive data or theoretical analysis. Includes compilations of significant scientific and technical data and information deemed to be of continuing reference value. NASA's counterpart of peer-reviewed formal professional papers but has less stringent limitations on manuscript length and extent of graphic presentations.

- TECHNICAL MEMORANDUM. Scientific and technical findings that are preliminary or of specialized interest, e.g., quick release reports, working papers, and bibliographies that contain minimal annotation. Does not contain extensive analysis.

- CONTRACTOR REPORT. Scientific and technical findings by NASA-sponsored contractors and grantees.

- CONFERENCE PUBLICATION. Collected papers from scientific and technical conferences, symposia, seminars, or other meetings sponsored or cosponsored by NASA.

- SPECIAL PUBLICATION. Scientific, technical, or historical information from NASA programs, projects, and mission, often concerned with subjects having substantial public interest.

- TECHNICAL TRANSLATION. English-language translations of foreign scientific and technical material pertinent to NASA's mission.

Specialized services that complement the STI Program Office's diverse offerings include creating custom thesauri, building customized databases, organizing and publishing research results ... even providing videos.

For more information about the NASA STI Program Office, see the following:

- Access the NASA STI Program Home Page at http://www.sti.nasa.gov/STI-homepage.html

- E-mail your question via the Internet to help@sti.nasa.gov

- Fax your question to the NASA Access Help Desk at (301) 621-0134

- Telephone the NASA Access Help Desk at (301) 621-0390

- Write to:
  NASA Access Help Desk
  NASA Center for AeroSpace Information
  7121 Standard Drive
  Hanover, MD 21076-1320

SeaWiFS Postlaunch Technical Report Series

Stanford B. Hooker, Editor
NASA Goddard Space Flight Center, Greenbelt, Maryland

Elaine R. Firestone, Senior Scientific Technical Editor
Science Applications International Corporation, Beltsville, Maryland

Volume 19, Coastal Atmosphere and Sea Time Series (CoASTS), Part 1: A Tower-Based, Long-Term Measurement Program

Giuseppe Zibordi, Jean-Françoise Berthon, John P. Doyle, Stefania Grossi, Dirk van der Linde, and Cristina Targa
JRC/SAI/Marine Environment Unit, Ispra, Italy

Luigi Alberotanza
CNR Institute for the Study of Dynamics of Large Masses, Venice, Italy

ISSN 1522-8789

G. Zibordi, J.-F. Berthon, J.P. Doyle, S. Grossi, D. van der Linde, C. Targa, and L. Alberotanza

ABSTRACT

The Coastal Atmosphere and Sea Time Series (CoASTS) Project, aimed at supporting ocean color research and applications, from 1995 up to the time of publication of this document, has ensured the collection of a comprehensive atmospheric and marine data set from an oceanographic tower located in the northern Adriatic Sea. The instruments and the measurement methodologies used to gather quantities relevant for bio-optical modeling and for the calibration and validation of ocean color sensors, are described. Particular emphasis is placed on four items: 1) the evaluation of perturbation effects in radiometric data (i.e., tower-shading, instrument self-shading, and bottom effects); 2) the intercomparison of seawater absorption coefficients from *in situ* measurements and from laboratory spectrometric analysis on discrete samples; 3) the intercomparison of two filter techniques for *in vivo* measurement of particulate absorption coefficients; and 4) the analysis of repeatability and reproducibility of the most relevant laboratory measurements carried out on seawater samples (i.e., particulate and yellow substance absorption coefficients, and pigment and total suspended matter concentrations). Sample data are also presented and discussed to illustrate the typical features characterizing the CoASTS measurement site in view of supporting the suitability of the CoASTS data set for bio-optical modeling and ocean color calibration and validation.

1. INTRODUCTION

Optical measurements from space enable estimates of the concentration of materials suspended or dissolved in seawater (i.e., pigment, sediment, and colored dissolved organic matter) which are of great relevance in environmental and climate-related studies. Because of this, a number of new advanced ocean color sensors were designed to support oceanographic studies and applications including the Modular Opto-electronic Sensor (MOS), the Ocean Color and Temperature Scanner (OCTS), the Polarization and Directionality of the Earth's Reflectance (POLDER) sensor, the Sea-viewing Wide Field-of-view Sensor (Sea-WiFS), the Moderate Resolution Imaging Spectroradiometer (MODIS), and the Medium Resolution Imaging Spectrometer (MERIS). All of these sensors were successfully launched and have contributed significantly to the general problem of inverting optical measurements to derive concentration estimates of biogeochemical parameters; several continue to provide regular coverage of the global biosphere.

To ensure a better exploitation of the data supplied by spaceborne sensors, national and international calibration and validation projects have been started. Their major objectives are the development of the bio-optical algorithms required for extracting quantitative information from space data; the validation of products obtained from satellite imagery; and the indirect absolute calibration (i.e., vicarious calibration) of the radiometers in space. All of these activities require comprehensive *in situ* atmospheric and marine measurements. In agreement with this requirement, the Coastal Atmosphere and Sea Time Series (CoASTS) Project was set up at the Joint Research Centre (JRC) in Ispra, Italy to support bio-optical modeling and ocean color calibration and validation exercises at a coastal site in the northern Adriatic Sea.

In order to provide a comprehensive overview of the CoASTS measurement activities, this report has three primary objectives:

1) Present the instrumentation and the measurement methodologies,

2) Assess the accuracy of the most relevant measurements needed for bio-optical modeling as well as ocean color vicarious calibration and algorithm validation activities; and

3) Discuss sample data that display the relevant features of the measurement site.

2. BACKGROUND

Ocean color calibration and validation activities carried out in the late 1970s and early 1980s for the Coastal Zone Color Scanner (CZCS), relied exclusively on a small number of ship-based campaigns for ground truth observations. More recent calibration and validation activities for MOS, OCTS, SeaWiFS, and MODIS make use of moored buoys, in addition to an extensive suite of oceanographic research cruises. Examples of radiometric buoy systems that were successfully deployed are as follows:

- The Yamato Bank Optical Mooring (YBOM), developed by the National Space Development Agency of Japan (NASDA) for OCTS calibration and validation (Kishino et al. 1997);

- The Marine Optical Buoy (MOBY), developed by the National Aeronautics and Space Administration (NASA) and the National Oceanographic and Atmospheric Administration (NOAA) to support Sea-WiFS and MODIS calibration and validation activities (Clark et al. 1997); and

1

■ The Plymouth Marine Bio-Optical Data Buoy (PlyMBODy), developed by the Plymouth Marine Laboratory (PML) in the United Kingdom for Sea-WiFS ocean color calibration and validation (Pinkerton and Aiken 1999).

More recently, a new European radiometric buoy is being deployed as part of the *Bouée pour l'acquisition de Séries Optiques à Long Terme*† (BOUSSOLE) Program (Antoine and Guevel 2000).

YBOM was equipped with a fluorometer, two pairs of upwelling radiance and downward irradiance sensors at 1.2 and 6.5 m depths providing spectral data from 400–800 nm, and an above-water irradiance reference sensor providing data at 860 nm. YBOM was first deployed and tested in the latter part of 1993, redeployed almost two years later for final testing, and operationally used during the Advanced Earth Observing Satellite (ADEOS-1) mission (Shimada et al. 1998).

The MOBY program became operational in July 1997 with three buoy systems supported by a deployment and refurbishment facility established at the University of Hawaii Marine Center in Honolulu. The buoy systems are deployed on a rotational basis off the coast of Lanai, Hawaii. The site is in the open ocean (low chlorophyll *a* concentration) with a constant aerosol type, and ensures availability of high resolution data throughout the SeaWiFS mission. MOBY is equipped with an above-water irradiance reference sensor and three pairs of downward irradiance and upwelling radiance collectors located at 2, 5, and 9 m depths, all providing data from 380–900 nm using custom-built hyperspectral sensors. The light sensors are mounted on arms to minimize the self-shading effect of the buoy, and orientation sensors allow the exclusion of data when the optical sensors are *behind* the buoy or excessively tilted. Mitigation of biofouling is accomplished with an aggressive campaign of diver visits to keep the optical windows clean. Coincident casts with an optical profiler are used to monitor data degradation between cleaning sessions and to independently demonstrate the baseline capabilities of the buoy data when the optical surfaces are not contaminated.

PlyMBODy was equipped with a conductivity, temperature, and depth (CTD) sensor; a fluorometer; an above-water irradiance reference sensor; and a pair of upwelling radiance sensors at 0.7 and 2.6 m depths. The radiometers were manufactured by Satlantic, Inc. (Halifax, Canada), and provided data in seven spectral bands from 412–780 nm. PlyMBODy was deployed off Plymouth in the English Channel, and was designed for a three-year lifetime from 1997–1999 (assuming a 9-month deployment from April–December). The full-scale beta version was deployed on site during a 3-month period (20 July to 20 October 2000), which allowed it to encounter a variety of meteorological situations. The buoy was equipped with

two inclinometers, a pressure sensor, an ARGOS beacon, and a flashing light. The goal of this deployment was to establish the capabilities of the buoy as well as to identify possible problems necessitating modifications.

The BOUSSOLE buoy will be deployed in the Ligurian Sea (between France and Corsica) in early 2002 as part of the MERIS calibration and validation activities being developed at *Laboratoire d'Océanographie de Villefranche* (LOV‡), located in Villefranche-sur-Mer, France. In terms of the optical measurements, the system consists of Satlantic radiometers measuring the solar irradiance (at 4.5 m above the surface), plus the downward irradiance, upward irradiance, and upwelling radiance at 4 and 9 m depths. The two-axis tilt, atmospheric pressure, and buoy orientation with respect to the sun, are also recorded. In addition, two fluorometers are mounted at 4 and 9 m, plus a transmissometer and a CTD are deployed at 9 m. Two sets of in-water optical sensors are used to minimize biofouling. While one set is in use, the other is characterized while fouled, cleaned, and then characterized again before redeployment—approximately one month after extraction by divers.

The use of buoys or ships has advantages and drawbacks. Moored buoys can easily ensure an almost continuous collection of a restricted set of parameters at a specific site. Alternatively, ship-based measurements can ensure a wide spatial data collection with a comprehensive optical and biogeochemical characterization of each sampling site, but with poor temporal resolution.

Recently, the use of oceanographic towers, as an alternative to buoy or shipboard measurements, was investigated (Zibordi et al. 1995 and Kearns et al. 1996). Compared to buoys, the use of offshore towers as mooring sites for continuous measurements has the disadvantage of increased contamination of the optical data with superstructure perturbations. The use of oceanographic towers as logistic platforms for comprehensive optical and biogeochemical measurements, when compared to ships, has the disadvantage of not permitting any spatial observation capability.

Despite the limitations, oceanographic towers offer the unique opportunity of a very stable measurement platform enabling easy and complete control of the deployment geometry (Hooker et al. 1999 and 2002). The latter feature may ensure the deployment of optical instruments with virtually no tilt and the exact identification of the solar illumination geometry needed for an accurate removal of superstructure shading effects (Zibordi et al. 1999). Taking advantage of these deployment conditions, the CoASTS Project has been relying on the use of the *Acqua Alta* Oceanographic Tower (AAOT) in the northern Adriatic Sea for the collection of a comprehensive atmospheric and

---

† Buoy for the acquisition of a long-term optical series.

‡ Formerly the *Laboratoire de Physique et Chimie Marines* (LPCM).

G. Zibordi, J.-F. Berthon, J.P. Doyle, S. Grossi, D. van der Linde, C. Targa, and L. Alberotanza
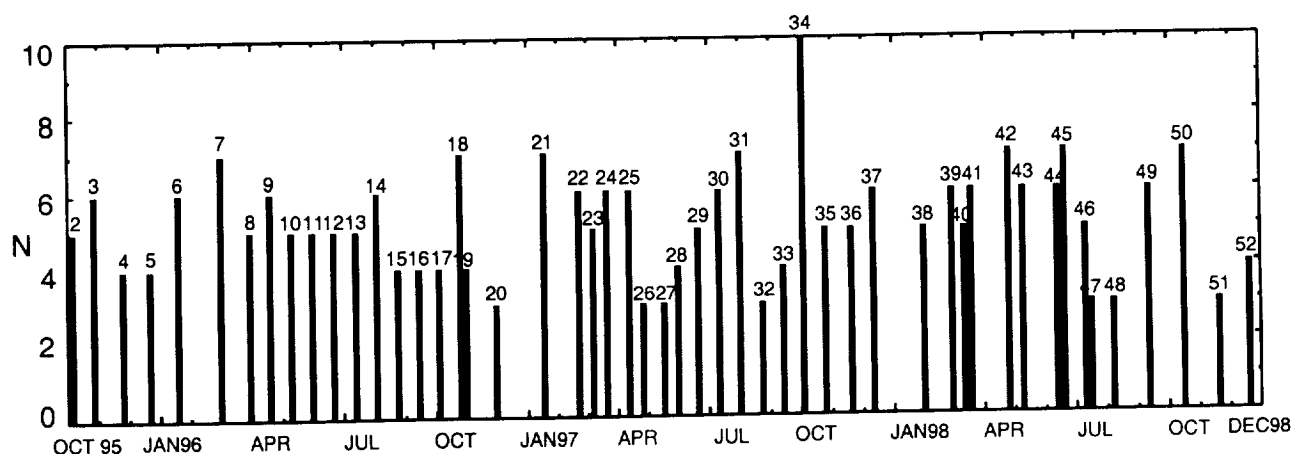

Fig. 1. The number of optical stations, N, performed in each CoASTS campaign (numbered sequentially above the bars) for the period October 1995–December 1998.

marine coastal data set. Periodic short deployments, using a modular in-water system that permits the removal of the light sensors in between measurement campaigns, will completely eliminate any biofouling of the in-water optical sensors.

3. COASTS OBJECTIVES

The CoASTS Project, started in 1995 and still continuing, has three aims:

1) The collection of the time series of atmospheric and marine data in the northern Adriatic Sea from a single measurement site for ocean color research and applications;

2) The analysis of the acquired data for the development of site- and seasonal-specific marine and atmospheric algorithms for ocean color data exploitation; and

3) The use of the acquired data in calibration and validation activities.

Recent studies (Berthon et al. 2000, Hooker et al. 2000a, Zibordi and Berthon 2001, Berthon et al. 2002, Sturm and Zibordi 2002, and Zibordi et al. 2002) have shown the capability of the project in reaching the former objectives and has clearly established the benefits offered by an ongoing time series of measurements (i.e., the continuous increase of the statistical significance of the data set for bio-optical modeling, and the expansion of the number of matchups for validation or vicarious calibration exercises).

4. MEASUREMENT PLAN

The CoASTS field campaigns, performed onboard the AAOT located 8 miles southeast off the Venice Lagoon (12.510°E,45.310°N), take place for a few days every 2–4 weeks. The frequency of campaigns is generally higher when biological phenomena are more pronounced (i.e., in the boreal spring and fall), and lower when environmental

effects decrease the likelihood of good optical data or safe embarkation onto the tower (i.e., during the boreal winter). Each comprehensive data collection—called a "station"— includes the in-water optical and hydrographic profiles, seawater samples at different depths (surface, 8 m, and 14 m), atmospheric optical measurements, meteorological data, and visual observations of cloud cover and sea state.

For each station, data and samples are generally collected in less than 30 min. Treatment of seawater samples (i.e., filtration and storage of samples in liquid nitrogen or in a refrigerator) generally requires 1–2 extra hours. Laboratory sample analysis is then performed within a few days of concluding the measurement campaign.

Figure 1 shows the number of campaigns and the number of stations per campaign starting in the latter part of 1995 and extending for three years. The number of stations per campaign, varying from a minimum of 3 up to a maximum of 10, is mostly determined by the meteorological conditions that may restrict the access to the tower or largely reduce the number of possible stations performed on ideal illumination conditions (i.e., when the sun is not covered by clouds or with an overcast sky).

5. SITE CHARACTERISTICS

The CoASTS site is located in a frontal region that can be characterized by Case-1 or Case-2 water types (Berthon et al. 2002). The Case-2 water characteristics are mostly determined by the input from the northern rivers (i.e., Piave, Livenza, and Tagliamento). The aerosol type, occasionally maritime, is mostly continental and is determined by atmospheric input from the nearby Po River valley. These characteristics of the site, represent most of the northern Adriatic Sea region.

The horizontal homogeneity in the vicinity of the measurement site, evaluated through SeaWiFS images, has displayed extremely different situations. The standard deviation of the satellite-derived normalized water-leaving ra-

Table 1. The typical average values of quantities characterizing the measurement site. The $\pm$ values indicate standard deviations.

Quantity	C_a $[\mu\text{g L}^{-1}]$	C_{TSM} $[\text{mg L}^{-1}]$	$K_{E_d}(490)$ $[\text{m}^{-1}]$	$a_{ys}(400)$ $[\text{m}^{-1}]$	$\tau_A(555)$
Average	1.3 ± 1.1	1.1 ± 0.7	0.21 ± 0.09	0.15 ± 0.06	0.14 ± 0.06

diance at 555 nm, $L_{WN}(555)$, computed from a 5×5 matrix of image pixels centered at the AAOT site, has shown values ranging from 0.02–0.66 (Sturm and Zibordi 2002) in the range of 0.5–$2.5 \,\text{mW cm}^{-2}\,\mu\text{m}^{-1}\,\text{sr}^{-1}$. This result indicates that at the measurement site, there are time periods characterized by high spatial inhomogeneity and other time periods characterized by high spatial uniformity. When the latter is the case, the AAOT *in situ* data can be assumed to be representative of the area surrounding the measurement site.

Table 1 presents the typical values of the most relevant quantities characterizing the CoASTS measurement site: the chlorophyll a concentration, C_a; the total suspended matter concentration, C_{TSM}; the diffuse attenuation coefficient for downwelling irradiance at 490 nm, K_{E_d}; the colored dissolved organic matter (CDOM) or "yellow substance" absorption coefficient, a_{ys}, at 400 nm; and the aerosol optical thickness, τ_a, at 555 nm.

6. THE AAOT

The AAOT, built in 1970, is owned by the *Istituto per lo Studio della Dinamica delle Grandi Masse*† (ISDGM) of the Italian National Research Council (CNR) in Venice. The AAOT, mounted on four grounded pillars, has four levels. Each level is 7.2 m×5.2 m in size with the exception of the lowest level which is $5.2 \,\text{m}^2$. Measurement activities are generally carried out on the second and fourth levels.

On the second level, at approximately 7 m above the sea surface, a portable laboratory provides space for treating water samples and for data logging. On the same level, an open grid platform 3.5 m wide, extends 6.5 m over the sea facing southeast; it also provides mounting points for the instruments to be deployed into the sea.

On the fourth level, at approximately 12 m above the sea surface, the meteorological and atmospheric optical instruments are installed. Electrical power is provided by diesel-powered generators and by lead-acid batteries. The generators provide electrical power during field campaigns when the AAOT is being used, and the batteries ensure power for the instruments used in continuous measurement programs.

7. THE MEASUREMENTS

The CoASTS data collection activities are split into field and laboratory work. The field measurements taken are composed of the following:

a) In-water, vertical profiles of spectral (z indicates depth and λ indicates wavelength) upwelling nadir radiance, $L_u(z, \lambda)$, downward irradiance, $E_d(z, \lambda)$, and upward irradiance, $E_u(z, \lambda)$, measured with the Wire-Stabilized Profiling Environmental Radiometer (WiSPER) composed of Satlantic components;

b) Above-water total solar irradiance, $E_d(0^+, \lambda)$, and diffuse sky irradiance, $E_i(0^+, \lambda)$, recorded with a Yankee Environmental Systems (YES), Inc. (Turners Falls, Massachusetts) MFR-6 rotating shadow band radiometer ($z = 0^+$ indicates an above-water measurement);

c) Direct solar irradiance, $E(\lambda)$, and diffuse sky radiance, $L_i(\theta, \phi, \lambda)$, at different zenith, θ, and azimuth, ϕ, angles in the almucantar and sun planes, taken with a CIMEL Electronique (Paris, France) CE-318 sun photometer;

d) Profiles of seawater beam attenuation, $c(z, \lambda)$, and absorption, $a(z, \lambda)$, coefficients, taken with a Western Environmental Technology Laboratories (WET-Labs), Inc. (Philomath, Oregon) AC-9; and

e) Ancillary field data (i.e., profiles of seawater temperature, $T_w(z)$, and salinity, $S_w(z)$; Secchi disk depth, SD; tide level, T_l; atmospheric pressure, P_a; relative humidity, RH; air temperature, T_a; wind speed, W_s, and direction, W_d; cloud cover, CC; and sea state, M).

The laboratory measurements, which provide data complementary to the field measurements, are:

- *In vivo* particulate absorption coefficient $a_p(\lambda)$ separated into its two components $a_{ph}(\lambda)$ for the pigmented and $a_{dp}(\lambda)$ for the nonpigmented matter, obtained from spectrometric analysis of particles retained on filters;

- CDOM absorption coefficient $a_{ys}(\lambda)$ obtained from spectrometric analysis of filtered seawater;

- Pigment concentration from high performance liquid chromatography (HPLC) analysis;

- Total suspended matter concentration, C_{TSM}, determined with the dry weighting technique; and

- Particle size distribution (PSD) spectra from Coulter Counter analysis.

In the collection of the CoASTS measurements, great effort was placed in ensuring consistency of data in a variety of ways:

1) Using assessed protocols for data collection, calibration, and preprocessing;

---

† The Institute for the Study of Dynamics of Large Masses.

2) Choosing data collection frequencies aimed at resolving seasonal variations in the observed quantities;

3) Assuring uniformity in the accuracy of the data over time; and

4) Attempting regular collection of each quantity included in the time series.

Most of the former *data consistency* elements, are easily achieved in a short-term measurement program, but over long periods (years) they can be affected by a number of elements:

- Old instruments being replaced by new instruments that have slightly different features (i.e., spectral response, sensitivity, or calibration uncertainties);

- Instrument failures temporarily interrupting specific measurements;

- Occasional harsh environmental conditions preventing regular data collection; and

- Revisions to the existing measurement protocols because of advances in the state of the art.

8. INSTRUMENTS AND METHODS

With the goal of highlighting the consistency of the CoASTS Project resulting from a multiyear data collection program, the following subsections describe the measurement methods and present the different quality control elements. The latter include, but are not limited to, absolute calibration accuracy, repeatability and reproducibility analysis, and intercomparison exercises. Particular importance is given to uncertainty analyses of radiometric marine quantities relevant for both bio-optical modeling and calibration and validation activities, i.e., $L_u(z, \lambda)$, $E_d(z, \lambda)$, and $E_u(z, \lambda)$.

8.1 Optical Measurements

In the following subsections, the instruments for in-water radiometric data collection are described together with the measurements and absolute calibration schemes, the techniques for subsurface values computation, and removal of tower-shading, self-shading, and bottom perturbations. An attempt is also made to quantify environmental effects (i.e., sea state, changes in seawater optical properties, and illumination conditions) on subsurface radiometric quantities.

8.1.1 Instruments and Measurement Methods

Measurements of $L_u(z, \lambda)$, $E_d(z, \lambda)$, and $E_u(z, \lambda)$ are obtained in seven spectral bands with a 10 nm bandwidth. The WiSPER system is installed on a metal frame which moves along two vertical wires fixed between the tower and the sea bottom (Fig. 2). The wires provide a high degree of stabilization of the WiSPER instrument system and prevent almost all movement out of the vertical plane.
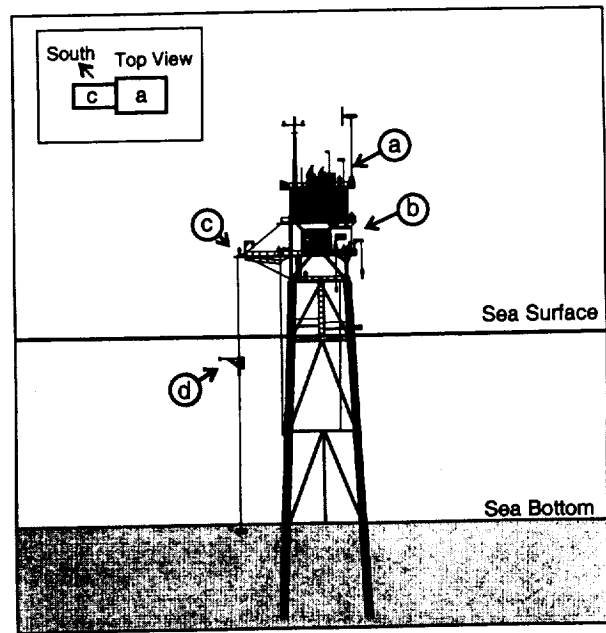

Fig. 2. A schematic of the AAOT showing the relevant items to the CoASTS program: a) the deployment platform for atmospheric instruments, b) the laboratory for water filtration and data logging, c) the deployment platform for in-water instruments, and d) the rig for in-water profiling instrumentation. The inset panel displays the AAOT top view.

The WiSPER radiometers are Satlantic Ocean Color Radiance and Irradiance series-200 sensors, OCR-200 and OCI-200, respectively. One OCR-200 is used to measure $L_u(z, \lambda)$, and one OCI-200 is used to measure $E_d(z, \lambda)$ and $E_u(z, \lambda)$, where $E_u(z, \lambda)$ is measured by rotating the bracket holding the OCI-200 for $E_d(z, \lambda)$ 180°. The light sensors are mounted on an extension boom, which places them 1 m away from the main part of the frame and approximately 7.5 m from the tower legs. Power, analog-to-digital (A/D) conversion, and telemetry of the light sensor data are provided by a Satlantic (16-bit) module called a DATA-100.

The effective signal-to-noise ratio (SNR) for $L_u(z, \lambda)$ in the spectral range 412–555 nm, is generally higher than 4×10^3, and more than 2×10^3 at 665 nm; the effective SNR for $E_d(z, \lambda)$ is generally greater than 10^4. Because the same OCI-200 is used for both $E_d(z, \lambda)$ and $E_u(z, \lambda)$, the effective SNR for $E_u(z, \lambda)$, only varies from $5-10 \times 10^2$ in the spectral range 412–555 nm, and is about 1.5×10^2 at 665 and 683 nm.

WiSPER, together with the AC-9 installed on the same rig to provide simultaneous measurements, is raised and lowered from the southeastern side of the tower by an electrical winch. The speed of the winch is approximately $0.1 \, \mathrm{m \, s^{-1}}$, which was chosen to satisfy the AC-9 deployment requirements (i.e., to have a water flux in the AC-9 measurement chambers ensuring the characterization of

Table 2. The nominal center wavelengths (in nanometers) for the channels of the *in situ* optical instruments used in the CoASTS Project.

Instrument and Channel	1	2	3	4	5	6	7	8	9
WiSPER† $L_u(z,\lambda)$	412	443	490	510	555	665	683		
WiSPER† $E_u(z,\lambda)$ and $E_d(z,\lambda)$	412	443	490	510	555	665	683		
AC-9 $a(z,\lambda)$ and $c(z,\lambda)$	412	440	488	510	555	630	650	676	715
MFR-6 $E_d(0^+,\lambda)$ and $E_i(0^+,\lambda)$	415	500	610	665	862	960			
CE-318 $L_i(\theta,\phi,\lambda)$				440	675	870	946	1020	
CE-318 $E(\lambda)$	340	380	440	501	675	870	1020		

† A Satlantic MVDS reference to measure $E_d(0^+,\lambda)$ with the same nominal center wavelengths was added in the second half of 1998.

seawater optical properties with a depth resolution better than 0.2 m).

During each measurement station, three sets of up-and-down profiles are made: the first and the third to collect $L_u(z,\lambda)$ and $E_d(z,\lambda)$, and the second to collect $L_u(z,\lambda)$ and $E_u(z,\lambda)$. Significant variations between quantities derived from the first and the third profile are used as an indicator of unstable environmental conditions. The second profile is primarily used to determine the Q-factor at nadir viewing:

$$Q_n(z,\lambda) = \frac{E_u(z,\lambda)}{L_u(z,\lambda)}. \qquad (1)$$

All of the collected data are automatically binned within the DATA-100 with a 0.2 m vertical resolution.

The major drawback of the applied methodology is the lack of continuous above-water irradiance measurements for minimizing the effects of illumination changes during casts. To overcome the former limitation, a Satlantic Multichannel Visible Detector System (MVDS) solar reference system was added to the instrumental set in the latter half of 1998. The MVDS provides continuous $E_d(0^+,\lambda)$ measurements at the same time of in-water profiling. Moreover, the WiSPER system was upgraded by adding a second OCI-200 to permit simultaneous measurements of $L_u(z,\lambda)$, $E_d(z,\lambda)$, and $E_u(z,\lambda)$. A summary of the optical instruments used in the CoASTS Project is given in Table 2.

The following work only deals with data collected up to the latter half of 1998 with the *two-sensor* WiSPER configuration, but most of the conclusions are applicable to the data collected with the *three-sensor* configuration without any loss in generality.

8.1.2 Absolute Calibration

The absolute calibration of the considered radiometric quantities is obtained from

$$\hat{\jmath}(z,\lambda) = \left[V_{\hat{\jmath}}(z,\lambda) - \bar{D}_{\hat{\jmath}}(\lambda)\right] C_{\hat{\jmath}}(\lambda) I_{\hat{\jmath}}(\lambda), \qquad (2)$$

where the "hat" notation (ˆ) indicates a measured quantity. The $\hat{\jmath}$ symbol (which is used both as a variable and a

subscript) indicates the calibrated radiometric quantities† $\hat{L}_u(z,\lambda)$, $\hat{E}_d(z,\lambda)$, and $\hat{E}_u(z,\lambda)$ (upwelled radiance, downward irradiance, and upward irradiance, respectively) not yet corrected for any perturbation effects (i.e., self-shading, tower-shading, and bottom). The digital voltage (in counts) at center wavelength λ and depth z is $V_{\hat{\jmath}}(z,\lambda)$, $\bar{D}_{\hat{\jmath}}(\lambda)$ is the average dark value (taken at the end of each measurement station by putting caps on the radiometers), $C_{\hat{\jmath}}(\lambda)$ is the absolute calibration coefficient, and $I_{\hat{\jmath}}(\lambda)$ is the immersion factor (i.e., the coefficient accounting for the change in sensor responsivity when the in-air calibration is applied to in-water measurements).

The absolute radiometric calibration coefficients— $C_{\hat{E}_u}(\lambda)$ and $C_{\hat{E}_d}(\lambda)$ [which are identical in the two-sensors WiSPER configuration, because of the use of the same radiometers for $\hat{E}_d(z,\lambda)$ and $\hat{E}_u(z,\lambda)$ measurements]—are determined using a 1,000 W FEL lamp traceable to the National Institute of Standards and Technology (NIST). The calibration coefficients $C_{\hat{L}_u}(\lambda)$ are determined making use of an FEL lamp and a Labsphere (Sutton, New Hampshire) 18 in Spectralon 99% reflectance plaque. In order to track any temporal change in the sensitivity of a light sensor, the calibration coefficients are generally determined every 3–6 measurement campaigns. When sensitivity changes larger than 1.5% are detected, a linear variation of the sensor sensitivity is assumed from one calibration date to the next as a function of the number of measurement campaigns falling within the two dates.

The uncertainty in the absolute calibration coefficients $C_{\hat{\jmath}}(\lambda)$ is ±2.1% for radiance (mostly resulting from the quadrature sum of the lamp calibration and plaque reflectance uncertainties, both taken equal to ±1.5%) and ±1.5% for irradiance (mostly due to the uncertainty in the lamp calibration values). These estimated values are confirmed by the detailed analyses of radiometric absolute calibration uncertainties presented by Hooker et al. (2002).

The immersion factors used in the calibration relationship are provided by the instrument manufacturer (in this

---

† For the CoASTS data set, radiance measurements are in units of $\mathrm{mW\,cm^{-2}\,\mu m^{-1}\,sr^{-1}}$ and irradiance measurements are in units of $\mathrm{mW\,cm^{-2}\,\mu m^{-1}}$.

case, Satlantic). The immersion factors for radiance sensors were computed theoretically following Mueller and Austin (1995), while the irradiance immersion factors were determined experimentally (S. McLean, pers. comm.). Because of the lack of independent and assessed data, the accuracy of immersion factors was assumed to be ±1% for radiance (mostly due to the uncertainty in the refractive index of the optical window) and ±3% for irradiance [using uncertainties estimated for cosine collectors made of the same material as the OCI-200 (Mueller 1995)].

In addition to uncertainties for $C_{\hat{\jmath}}(\lambda)$ and $I_{\hat{\jmath}}(\lambda)$, the non-ideal cosine response of the irradiance collectors could be a further source of uncertainty in irradiance measurements. In the specific case of the OCI-200 radiometers, the non-cosine response may cause slightly different uncertainties at different wavelengths because of the use of separate collectors for each radiometric channel. The Sea-WiFS measurement protocol (Mueller and Austin 1995) requires the uncertainty in the irradiance measurement of a collimated light to be better than 2% for angles from 0–65° with respect to the optical axis, and within 10% for angles from 65–90°. Because of the unavailability of published data on the accuracy of the cosine response for Satlantic OCI-200 radiometers, a ±2% uncertainty is assumed at all wavelengths.

The uncertainties for $C_{\hat{\jmath}}(\lambda)$, $I_{\hat{\jmath}}(\lambda)$, and the cosine response of irradiance sensors, lead to a quadrature sum of ±2.3% and ±3.9% for the overall radiance and irradiance uncertainty values, respectively.

8.1.3 Computation of Subsurface Values

A subsurface value† $\hat{\jmath}(0^-, \lambda)$ [i.e., $\hat{L}_u(0^-, \lambda)$, $\hat{E}_d(0^-, \lambda)$ and $\hat{E}_u(0^-, \lambda)$] is the exponent of the intercept from the least-squares linear regression of $\ln(\hat{\jmath}(z, \lambda))$ versus depth within a near-surface interval $z_0 < z < z_1$, where $\ln(\hat{\jmath}(z, \lambda))$ is either $\ln(\hat{L}_u(z, \lambda))$, $\ln(\hat{E}_d(z, \lambda))$, or $\ln(\hat{E}_u(z, \lambda))$. Depths z_0 and z_1 are iteratively chosen (D'Alimonte et al. 2001) to satisfy the requirement of a linear decay in $\ln\hat{\jmath}(z, \lambda)$ as a function of z (generally for the CoASTS stations $0.3 < z_0 < 1$ m and $2.5 < z_1 < 4.5$ m). The negative value of the slope of the regression fit is the diffuse attenuation coefficient $K_{\hat{\jmath}}(\lambda)$ [i.e., $K_{\hat{L}_u}(\lambda)$, $K_{\hat{E}_u}(\lambda)$ and $K_{\hat{E}_d}(\lambda)$].

The subsurface values are corrected for perturbation effects according to

$$L_u(0^-, \lambda) = \hat{L}_u(0^-, \lambda)\, \eta_{\hat{L}_u}^{TS}(\lambda)\, \eta_{\hat{L}_u}^{SS}(\lambda)\, \eta_{\hat{L}_u}^{BE}(\lambda), \quad (3)$$

$$E_d(0^-, \lambda) = \hat{E}_d(0^-, \lambda)\, \eta_{\hat{E}_d}^{TS}(\lambda), \quad (4)$$

and

$$E_u(0^-, \lambda) = \hat{E}_u(0^-, \lambda)\, \eta_{\hat{E}_u}^{TS}(\lambda)\, \eta_{\hat{E}_u}^{SS}(\lambda)\, \eta_{\hat{E}_u}^{BE}(\lambda), \quad (5)$$

---

† A depth immediately below the sea surface is indicated by $z = 0^-$.

where $L_u(0^-, \lambda)$, $E_d(0^-, \lambda)$, and $E_u(0^-, \lambda)$ are the corrected values, and $\eta_{\hat{\jmath}}^{TS}(\lambda)$, $\eta_{\hat{\jmath}}^{SS}(\lambda)$, and $\eta_{\hat{\jmath}}^{BE}(\lambda)$ are the tower-shading, self-shading, and bottom effects correction factors, respectively.

The application of the correction factors in (3)–(5) assumes the sources of the perturbations are all independent. The accuracy of the corrections is also based on the assumptions that the tower-shading and self-shading effects are depth independent, and the bottom effects are weak. Because $\hat{L}_u(0^-, \lambda)$, $\hat{E}_d(0^-, \lambda)$, and $\hat{E}_u(0^-, \lambda)$ are all computed from subsurface data (generally within the 0.3–4.5 m depth interval) and bottom effects are, in most of the cases, less than 2% of the signal at $z = 0^-$, the correction formulations given in (3)–(5) can be applied to most of the CoASTS stations.

The factor $\eta_{\hat{\jmath}}$ associated with each perturbation effect is defined as

$$\eta_{\hat{\jmath}}(\lambda) = \frac{\hat{\jmath}(0^-, \lambda)}{\jmath(0^-, \lambda)}, \quad (6)$$

where $\hat{\jmath}(0^-, \lambda)$ is the measured radiometric quantity and $\jmath(0^-, \lambda)$ is the corrected value [i.e., $L_u(0^-, \lambda)$, $E_d(0^-, \lambda)$, and $E_u(0^-, \lambda)$].

The uncertainties related to perturbations discussed in this document, make reference to data taken during so-called *clear-sun*, *clear-sky*, and *almost-stable* environmental conditions. During clear-sun conditions, there are no clouds in front of, or in near proximity of, the solar disc. During clear-sky conditions, the sky is cloudless (except perhaps at the horizon). Clear-sun and clear-sky conditions are discriminated by a threshold for the ratio between above-water diffuse and direct irradiance at 412 nm, $r_i(412)$, obtained from the MFR-6 data measured at the same time as the in-water optical profiles; the threshold used for data processing purposes is $r_i(412) \leq 2.0$. Almost-stable environmental conditions are identified by differences lower than 10% between the $L_u(0^-, \lambda)/E_d(0^-, \lambda)$ ratios computed from successive radiometric profiles (i.e., the first and the third) taken in each measurement station.

Figure 3 shows the temporal evolution of the total correction factors $\eta_{\hat{L}_u}^{TS}(\lambda)\,\eta_{\hat{L}_u}^{SS}(\lambda)\,\eta_{\hat{L}_u}^{BE}(\lambda)$ applied to $\hat{L}_u(0^-, \lambda)$ and the frequency distribution of the related percentage values $100[\eta_{\hat{L}_u}^{TS}(\lambda)\,\eta_{\hat{L}_u}^{SS}(\lambda)\,\eta_{\hat{L}_u}^{BE}(\lambda) - 1]$ at 412, 490, 555, and 665 nm (where the latter wavelengths were chosen to ensure that the correction factors are represented over the visible spectrum). The total correction factors exhibit significant spectral dependence and very large variations at all wavelengths, with minimum values ranging from 0.91–1.10 at 555 nm, and maximum values ranging from 1.06–1.16 at 665 nm. The frequency distribution of percentage corrections shows average values of 9.2, 5.5, 3.2, and 9.3% at 412, 490, 555, and 665 nm, respectively. The former results highlight the spectral and seasonal dependence of perturbation effects which, if not removed, can induce significant inconsistencies in the time series of $L_u(0^-, \lambda)$, $E_d(0^-, \lambda)$, and $E_u(0^-, \lambda)$.
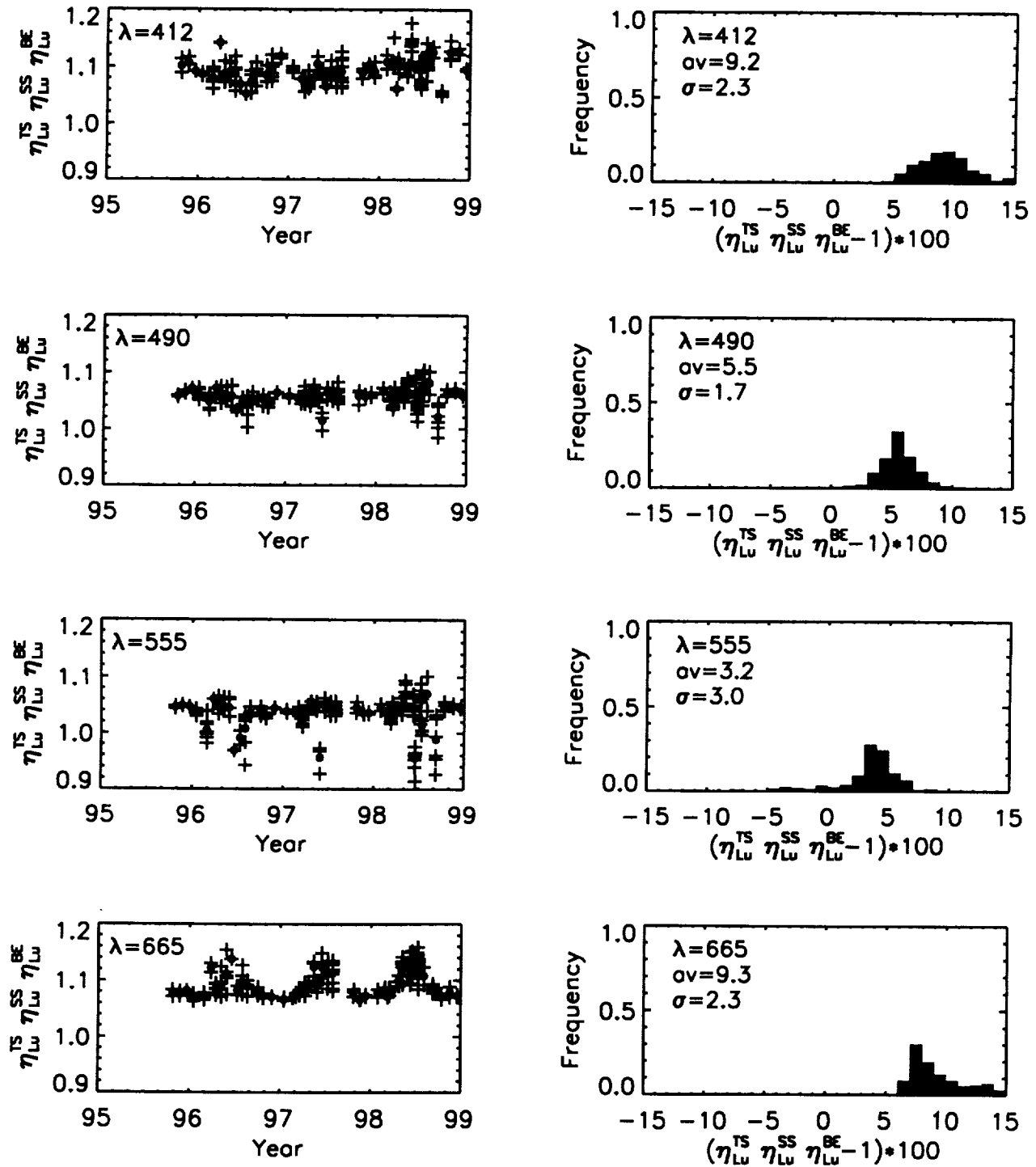
Fig. 3. The total correction factors for tower-shading, self-shading, and bottom effects $\eta_{L_u}^{TS}(\lambda)\,\eta_{L_u}^{SS}(\lambda)\,\eta_{L_u}^{BE}(\lambda)$ applied to upwelling radiance as a function of the station date at $\lambda = 412, 490, 555, 665\,\mathrm{nm}$, and the related percentage frequency distribution $[\eta_{\hat{E}_u}^{TS}(\lambda)\,\eta_{\hat{E}_u}^{SS}(\lambda)\,\eta_{\hat{E}_u}^{BE}(\lambda) - 1]\,100$. The plus symbol (+) indicates single station values, while the dot symbol (•) indicates mean campaign values. The average is indicated as av, and σ is the standard deviation. The number of points is $n = 215$.

Table 3. The reference values used for computing the tower-shading correction factors at each OCI-200 and OCR-200 nominal center wavelength (given in units of nanometers) for $L_u(0^-, \lambda)$, $E_u(0^-, \lambda)$, and $E_d(0^-, \lambda)$.

Index	412	443	490	510	555	665
a $[\text{m}^{-1}]$	0.02	0.05	0.10	0.30	0.50	
ω_0	0.50	0.70	0.80	0.85	0.90	0.95
θ_0 $[°]$	25	30	40	50	60	70
ϕ_0 $[°]$	90	135	180	225	270	
τ_a	0.00	0.05	0.10	0.50	1.00	$\rightarrow \infty$

Table 4. The OCI-200 and OCR-200 wavelength-specific values used for computing tower-shading correction factors (the wavelengths are given in units of nanometers).

Parameter	412	443	490	510	555	665
ρ_B	1.3×10^{-2}	1.8×10^{-2}	3.1×10^{-2}	4.0×10^{-2}	6.1×10^{-2}	26.6×10^{-2}
τ_o	6.6×10^{-4}	1.0×10^{-3}	7.4×10^{-3}	1.4×10^{-2}	3.3×10^{-2}	1.7×10^{-2}
τ_R	0.32	0.24	0.16	0.13	0.09	0.04

The methods applied for the removal of the different perturbation sources are briefly discussed in the following section.

8.1.4 Estimate of Measurement Perturbations

The tower-shading correction factors $\eta_{L_u}^{TS}(\lambda)$, $\eta_{E_u}^{TS}(\lambda)$, and $\eta_{E_d}^{TS}(\lambda)$ were computed using a Monte Carlo modeling of the radiance and irradiance fields at the AAOT site for the specific point and geometry where the WiSPER measurements were taken. Modeling results were validated through field data obtained from an experiment specifically designed to quantify $L_u(z, \lambda)$ and $E_d(z, \lambda)$ tower-shading effects as a function of the distance from the tower (Zibordi et al. 1999).

The operational tower-shading corrections (Doyle and Zibordi 2002) were performed making use of look-up tables (LUTs) in which the correction factors for each center wavelength are indexed by discrete values of:

- The solar zenith and azimuth angles, θ_0 and ϕ_0, respectively;
- The total seawater absorption, $a(\lambda)$;
- The seawater single scattering albedo, defined as $\omega_0(\lambda) = b(\lambda)/[a(\lambda) + b(\lambda)]$, where $b(\lambda)$ is the total seawater scattering coeffficient; and
- The above-water diffuse over direct irradiance ratio, $r_i(\lambda)$.

In building the LUTs, the variability in $r_i(\lambda)$ was produced by simulating the tower-shading uncertainties during clear-sky conditions with different values of the aerosol optical thickness, $\tau_a(\lambda)$. The overcast sky condition was simulated as a special case by assuming a totally isotropic sky illumination, i.e., equivalent to the light field resulting from $\tau_a(\lambda) \rightarrow \infty$.

Table 3 presents the discrete reference values θ_0, ϕ_0, $a(\lambda)$, $\omega_0(\lambda)$, and $\tau_a(\lambda)$ used for computing the LUTs for

the tower-shading correction scheme. The OCI-200 and OCR-200 wavelength-dependent values for the bottom reflectance $\rho_B(\lambda)$, Rayleigh (molecular scattering) optical thickness $\tau_R(\lambda)$, and ozone optical thickness $\tau_o(\lambda)$, are given in Table 4. The discrete reference values shown in Table 3 were chosen based on the representative variability of the related quantities measured at the AAOT site.

The $a(\lambda)$ values used for retrieving correction factors from the LUTs are computed from AC-9 measurements or, as an alternative when AC-9 data are not available, obtained from discrete surface seawater samples. Similarly, the $b(\lambda)$ values are computed from AC-9 measurements or, as an alternative, estimated from the subsurface irradiance reflectance, $\hat{R}(0^-, \lambda) = \hat{E}_u(0^-, \lambda)/\hat{E}_d(0^-, \lambda)$, using the relationship suggested by Kirk (1994):

$$b(\lambda) = a(\lambda) \frac{103 \, \hat{R}(0^-, \lambda)}{1 - \hat{R}(0^-, \lambda)}, \qquad (7)$$

where the tower-shading, self-shading, and bottom effects on $\hat{R}(0^-, \lambda)$ are neglected.

The possible sources of uncertainties in the correction scheme for removing tower-shading effects, some of which might be significant under certain circumstances, are as follows:

1) Assuming the tower structure absorbs all incident photons (i.e., the tower is perfectly black and does not reflect any light);

2) Neglecting roughness in modeling the sea surface reflectance; and

3) Using correction factors computed for discrete values of the input variables θ_0, ϕ_0, $a(\lambda)$, $\omega_0(\lambda)$, and $\tau_a(\lambda)$ without any interpolation.

The instrument self-shading correction factors $\eta_{L_u}^{SS}(\lambda)$ and $\eta_{E_u}^{SS}(\lambda)$ are computed using the scheme proposed by

Gordon and Ding (1992) plus the parameterizations suggested by Zibordi and Ferrari (1995) and Mueller and Austin (1995). Setting the OCI-200 and OCR-200 instrument radius $R_I = 4.5$ cm and the radius of the sensor entrance optics $R_S = 0.5$ cm, the computation of the self-shading correction factors is made using the following data:

a) The average θ_0 of each cast;

b) $a(\lambda)$ computed from AC-9 measurements or as an alternative (when AC-9 data are not available) obtained from surface seawater samples; and

c) $r_i(\lambda)$ from the MFR-6 data taken at the same time as the in-water optical profiles.

Possible sources of uncertainties in the computation of $\eta_{\hat{L}_u}^{SS}(\lambda)$ and $\eta_{\hat{E}_u}^{SS}(\lambda)$ include the following:

- Assuming the instrument as an ideal disc instead of a cylinder;

- Assuming each channel sensor is located at the center of the instrument (they are actually arranged in a circle with one channel in the center); and

- Neglecting the roughness of the sea surface.

The correction factors $\eta_{\hat{E}_u}^{BE}(\lambda)$ and $\eta_{\hat{L}_u}^{BE}(\lambda)$ for bottom (sand and mud at approximately 17 m depth), are computed making use of a simple analytical model derived from Maritorena et al. (1994) for bottom correction of irradiance reflectance. The model requires the so-called *operational* diffuse attenuation coefficient, $\bar{K}_{E_d}(\lambda)$, which is assumed here to be equal to the average diffuse attenuation coefficient obtained from the linear regression of $\ln\left[\hat{E}_d(z,\lambda)\right]$ versus depth between the surface and the bottom depth, z_B. Another needed parameter is the bottom reflectance, $\rho_B(\lambda)$, which is given by

$$\rho_B(\lambda) = \frac{\hat{E}_u(z_B,\lambda)}{\hat{E}_d(z_B,\lambda)}, \quad (8)$$

where $\hat{E}_u(z_B,\lambda)$ and $\hat{E}_d(z_B,\lambda)$ are the extrapolated values of $\hat{E}_u(z,\lambda)$ and $\hat{E}_d(z,\lambda)$ at the bottom depth z_B (the mean $\rho_B(\lambda)$ values at the AAOT site are listed in Table 4).

The bottom-corrected upward irradiance just below the surface is given by

$$E_u^{BE}(0^-,\lambda) = \frac{1}{1-k(z_B,\lambda)}\left[\hat{E}_u(0^-,\lambda)\right.$$
$$\left. - \rho_B(\lambda)\,\hat{E}_d(0^-,\lambda)\,k(z_B,\lambda)\right], \quad (9)$$

where $k(z_B,\lambda)$ is the transmittance for the downward plus upward normal optical paths beween the surface and the bottom at depth z_B and is equivalent to

$$k(z_B,\lambda) = \exp\left[-2\,\bar{K}_{E_d}(\lambda)\,z_B\right]. \quad (10)$$

Similar to $E_u^{BE}(0^-,\lambda)$, the bottom-corrected upward radiance $L_u^{BE}(0^-,\lambda)$ is estimated by:

$$L_u^{BE}(0^-,\lambda) = \left[\hat{L}_u(0^-,\lambda)\right.$$
$$\left. - \frac{\rho_B(\lambda)\hat{E}_d(0^-,\lambda)k(z_B,\lambda)}{\hat{Q}_n(0^-,\lambda)}\right], \quad (11)$$

where, as given in (1), $\hat{Q}_n(0^-,\lambda) = \hat{E}_u(0^-,\lambda)/\hat{L}_u(0^-,\lambda)$ in units of steradians. The former relationship assumes $\hat{Q}_n(0^-,\lambda)$ is not affected by bottom effects, i.e., $\hat{E}_u(0^-,\lambda)$ and $\hat{L}_u(0^-,\lambda)$ are identically affected by the bottom. Even though this assumption is only valid in isotropic conditions [i.e., when $\hat{Q}_n(0^-,\lambda) = \pi$ sr and the bottom reflectance $\rho_B(\lambda)$ is lambertian] it can be shown that in the worst conditions observed in the entire CoASTS data set (i.e., with $\eta_{\hat{L}_u}^{BE}(\lambda) \approx 0.9$), an extreme uncertainty of $\pm 10\%$ in $\hat{Q}_n(0^-,\lambda)$ induces a variation of approximately $\pm 0.5\%$ in $L_u^{BE}(0^-,\lambda)$.

Uncertainties in the computation of $\eta_{\hat{L}_u}^{BE}(\lambda)$ and $\eta_{\hat{E}_u}^{BE}(\lambda)$ are induced by:

a) Applying a simple (approximate) analytical model;

b) Using the operational diffuse attenuation coefficient; and

c) Assuming the bottom reflectance is lambertian.

8.1.5 Environmental Effects

To complete the analysis on radiometric quantities, the uncertainties due to surface roughness, changes in seawater characteristics, and variability in the illumination conditions during the in-water optical profiling are investigated. These uncertainties are estimated for $L_u(0^-,\lambda)$ and $E_d(0^-,\lambda)$ using data taken during clear-sun conditions, with wind speeds less than $5\,\mathrm{m\,s^{-1}}$ (the typical circumstance for CoASTS measurements), and at a time close to local noon (to minimize variations in illumination conditions caused by changes in the solar zenith angle).

Using 19 stations that fulfill the aforementioned conditions, the uncertainty attributed to environmental effects was estimated from the average absolute percent difference† (APD) between $L_u(0^-,\lambda)$ values, and between $E_d(0^-,\lambda)$ values, computed from successive profiles (i.e., the first and the third profile of each measurement station) about 20 min apart. Results for $L_u(0^-,\lambda)$ show average APDs ranging from $2.7 \pm 3.1\%$ to $3.2 \pm 2.9\%$ at 412 and 665 nm, respectively. Similarly, results for $E_d(0^-,\lambda)$ show average APDs ranging from $1.9 \pm 1.7\%$ to $3.0 \pm 2.3\%$ at the same wavelengths. The former relatively low values are probably the consequence of two factors:

---

† The APD between two quantities, X and Y, is defined as $200|X-Y|/(X+Y)$.

Table 5. Average values of $r_i(\lambda)$ measured at the AAOT site during clear-sun conditions. The standard deviations are indicated by the "$\pm$" sign.

λ [nm]	412	443	490	510	555	665
Average	0.89 ± 0.41	0.73 ± 0.35	0.53 ± 0.27	0.46 ± 0.24	0.34 ± 0.19	0.23 ± 0.14

a) The high stability of the deployment system, which prevents any sensor tilts; and

b) The low winch deployment speed ($0.1\,\mathrm{m\,s^{-1}}$), which ensures at least 60 samples per meter for the averaging of surface perturbations in the profile data.

8.2 $E_d(0^+,\lambda)$ and $E_i(0^+,\lambda)$ Measurements

Total and diffuse above-water solar irradiances are measured using the MFR-6 automatic radiometer (Harrison et al. 1994). Measurements are performed in six bands 10 nm wide (Table 2) and in one broad band (ranging from approximately 400–1,100 nm). The total and diffuse components are measured by alternately exposing and shading the cosine collector of the instrument. The collector shading from the direct sun component is obtained through an automated arc-shaped (shadow) band moving above the center of the entrance aperture, which blocks a portion of the sky with a 3.3° angle.

Each measurement sequence includes four independent measurements:

- $E_d(0^+,\lambda)$ taken with the band at its home (i.e., nadir) position;
- $\hat{E}_i(0^+,\lambda)$ with the sun blocked by the band;
- Two more measurements taken when the band is positioned 9° to either side of the sun.

The latter two measurements are automatically used by the system firmware to compute $E_i(0^+,\lambda)$ by correcting $\hat{E}_i(0^+,\lambda)$ for the sky radiance blocked by the band when the sun and a portion of the sky are occulted. The system automatically performs a maximum of three sequences of measurements per minute.

In the framework of the CoASTS campaigns, MFR-6 data were taken at 10 min intervals during each measurement station. The data, used to estimate $r_i(\lambda)$ for self-shading and tower-shading corrections, are computed according to

$$r_i(\lambda) = \frac{E_i(0^+,\lambda)}{E_d(0^+,\lambda) - E_i(0^+,\lambda)}. \quad (12)$$

Because $E_d(0^+,\lambda)$ and $E_i(0^+,\lambda)$ are measured with the same instrument, an absolute radiometric calibration of the instrument is not required. Table 5 gives the values for $r_i(\lambda)$ measured at the same time as the in-water optical data during clear-sun conditions for the 1995–1998 period. Under fully cloudy conditions, $r_i(\lambda) \to \infty$.

8.3 $E_s(\lambda)$ and $L_i(\theta,\phi,\lambda)$ Measurements

The direct normal sun irradiance, $E_s(\lambda)$ and the diffuse sky radiance, in a wide range of angles in the almucantar and sun planes, are both measured with a CE-318 automatic sun photometer. The device is composed of:

1) A sensor installed in an alto-azimuthal platform;

2) A programmable unit controlling the measurement sequences, sun–sky pointing, and data logging; and

3) A data transmission unit based on the Meteorological Satellite (METEOSAT) Data Collection Platform (DCP) system.

The optical part of the CE-318 is composed of two collimators with a 1.2° full-angle field of view [one is used for $L_i(\theta,\phi,\lambda)$ and the other is used for both $E(\lambda)$ and $L_i(\theta,\phi,\lambda)$ in the sun aureole], and a filter wheel with eight filters. The direct normal sun irradiance, used for the retrieval of the aerosol optical thickness, is taken at regular air mass intervals in all spectral channels. The diffuse sky radiance, mainly used for the retrieval of the aerosol particle size distribution and phase function (Holben et al. 1998), is only taken for channels in the 440–1,020 nm range (Table 2). The CE-318 installed on the AAOT, is part of the Aerosol Robotic Network (AERONET) at the NASA Goddard Space Flight Center (GSFC) where the regular instrument calibrations occur, as well as the almost near-real time data processing and data quality assurance (Holben et al. 1998).

Instrument calibrations for $L_i(\theta,\phi,\lambda)$ data were performed by the AERONET project using a 2 m integrating sphere. The uncertainty in the absolute radiometric calibration of $L_i(\theta,\phi,\lambda)$ is assumed to be within $\pm 4\%$. Instrument calibrations for $E(\lambda)$ data were carried out through intercalibration with a reference sun photometer regularly calibrated at the high altitude Mauna Loa Observatory (Hilo, Hawaii) with the Langley technique (Holben et al. 1998).

The calibrated sun photometer data $E(\lambda)$, assuming no water vapor absorption, are related to the atmospheric optical thickness, τ, through

$$E(\lambda) = E_0(\lambda)D_y \exp[-\tau(\lambda)\,m], \quad (13)$$

where $E_0(\lambda)$ is the extra atmospheric irradiance, D_y is the sequential day of the year (which accounts for the sun–Earth distance), $\tau = \tau_R + \tau_o + \tau_a$ (i.e., the sum of the molecular, ozone, and aerosol optical thicknesses, respectively), and m is the relative air mass. Assuming the instrument

is properly calibrated, the uncertainty associated with the retrieved τ_a is estimated to be less than 0.02 (Smirnov et al. 2000).

Results from Langley calibrations of $E(\lambda)$ data taken at the AAOT on clear and atmospherically stable days, have shown differences generally lower than $\pm 2\%$ with respect to the calibrations performed by GSFC in the 440–1,020 nm spectral range. This result supports the concept of using clear and stable days for making on-site field checks of the stability of the absolute radiometric calibration.

8.4 $c(z,\lambda)$ and $a(z,\lambda)$ Measurements

The beam attenuation $c(z, \lambda)$ and absorption $a(z, \lambda)$ coefficients of seawater (both in units of per meter) are computed from measurements taken in nine bands (Table 2), 10 nm wide, with a 25 cm pathlength AC-9 equipped with a Sea-Bird Electronics (Bellevue, Washington) 5T submersible pump for constant water flow. The calibrated beam attenuation and absorption coefficients, $\hat{c}_{t-w}(z, \lambda)$ and $\hat{a}_{t-w}(z, \lambda)$, respectively, are obtained from the AC-9 measurements for suspended and dissolved optical components (not including the contribution of pure seawater). Both of these parameters are then corrected for temperature, T_w, and salinity, S_w, differences between the *in situ* seawater and the pure water used for laboratory calibration (following the methodology recommended in an internal document by WETLabs, the instrument manufacturer, with CTD profile data taken at the same time as the AC-9 measurements).

While $\hat{c}_{t-w}^{ST}(z, \lambda)$—the measured beam attenuation coefficient corrected for salinity and temperature effects— does not require any further processing [i.e., $c(z, \lambda) = \hat{c}_{t-w}^{ST}(z, \lambda) + c_w(\lambda)$, where $c_w(\lambda)$ is the pure seawater beam attenuation coefficient], the resulting salinity and temperature corrected $\hat{a}_{t-w}^{ST}(z, \lambda)$ data need to be further corrected for scattering effects to retrieve $a(z, \lambda)$. The latter scattering effects, due to the finite acceptance angle of the optics and to the incompletely reflective surface of the absorption chamber (which prevents the detector from collecting all the scattered light), induces overestimates of the retrieved absorption coefficient.

The WETLabs suggestions for correcting the absorption data for scattering effects, recounted here for completeness, are based on three methods:

1. The removal at each wavelength of the measured absorption coefficient at a reference wavelength, λ_0, in the near infrared part of the spectrum (usually $\lambda_0 = 715$ nm) where the absorption by particulate matter and colored dissolved organic matter is assumed to be zero:

$$a(z,\lambda) = \hat{a}_{t-w}^{ST}(z,\lambda) + a_w(\lambda) - \hat{a}_{t-w}^{ST}(z,\lambda_0), \quad (14)$$

where $a_w(\lambda)$ (in units of per meter) is the pure seawater absorption (Pope and Fry 1997).

2. The removal of a fixed percentage, δ (which is independent of λ and typically varying from 0.14–0.18), of the scattering coefficient $b_{t-w}(z, \lambda) = c_{t-w}(z, \lambda) - a_{t-w}(z, \lambda)$, by assuming that the shape of the volume scattering function is independent of λ and of the type of particulate material:

$$\begin{aligned} a(z,\lambda) &= \hat{a}_{t-w}^{ST}(z,\lambda) + a_w(\lambda) \\ &\quad - \delta\left[\hat{c}_{t-w}^{ST}(z,\lambda) - \hat{a}_{t-w}^{ST}(z,\lambda)\right]. \end{aligned} \quad (15)$$

3. The removal of a variable percentage of the scattering coefficient $b_{t-w}(z, \lambda)$ estimated from $\hat{c}_{t-w}^{ST}(z, \lambda)$ and $\hat{a}_{t-w}^{ST}(z, \lambda)$ at λ and λ_0, by assuming that the absorption coefficient of particulate and dissolved material is zero at the reference wavelength $\lambda_0 = 715$ nm and that the shape of the volume scattering function is independent of wavelength (Zaneveld et al. 1994):

$$\begin{aligned} a(z,\lambda) &= \hat{a}_{t-w}^{ST}(z,\lambda) + a_w(\lambda) \\ &\quad - \frac{\hat{a}_{t-w}^{ST}(z,\lambda_0)\left[\hat{c}_{t-w}^{ST}(z,\lambda) - \hat{a}_{t-w}^{ST}(z,\lambda)\right]}{\hat{c}_{t-w}^{ST}(z,\lambda_0) - \hat{a}_{t-w}^{ST}(z,\lambda_0)}. \end{aligned} \quad (16)$$

In Fig. 4, an intercomparison is given between the sum of the absorption coefficients obtained from discrete seawater samples (Sects. 8.6 and 8.7), $a_{ph}(z, \lambda) + a_{dp}(z, \lambda) + a_{ys}(z, \lambda)$, and the absorption coefficients computed from the AC-9 data corrected for scattering effects according to method 3 above, $a_{t-w}(z, \lambda) = a(z, \lambda) - a_w(z, \lambda)$. The intercomparisons are given for the 412, 488, 555, and 676 nm wavelengths, at depths $z=1$, 8, and 14 m for which absorption coefficients from the AC-9 and seawater discrete samples are both available. The AC-9 values are for data binned with a 1 m depth resolution. The agreement between $a_{ph}(z, \lambda) + a_{dp}(z, \lambda) + a_{ys}(z, \lambda)$ and $a_{t-w}(z, \lambda)$, is very good at 412 nm, but a general underestimate of the absorption is noticed at 488, 555, and 676 nm with the worst results at 510 nm (not shown here), which exhibit average percent differences of 25%.

The absolute calibration of the AC-9 was performed by WETLabs. Additional calibrations were periodically performed in the laboratory using clean (Milli-Q†) water. Offsets between the original WETLabs and laboratory calibrations were used for correcting $c_{t-w}(z, \lambda)$ and $a_{t-w}(z, \lambda)$ measurements by drifts due to changes in instrument sensitivity. The former clean-water calibrations showed offsets slightly drifting over the measurement period and exhibiting values generally from 0.08–0.14 m^{-1} for $c_{t-w}(z, \lambda)$, and from 0.005–0.07 m^{-1} for $a_{t-w}(z, \lambda)$ in the spectral range 412–715 nm. Recent work on AC-9 calibration (Twardowski et al. 1999), has shown the need for daily clean-water calibrations. Because of this, it may result that

---

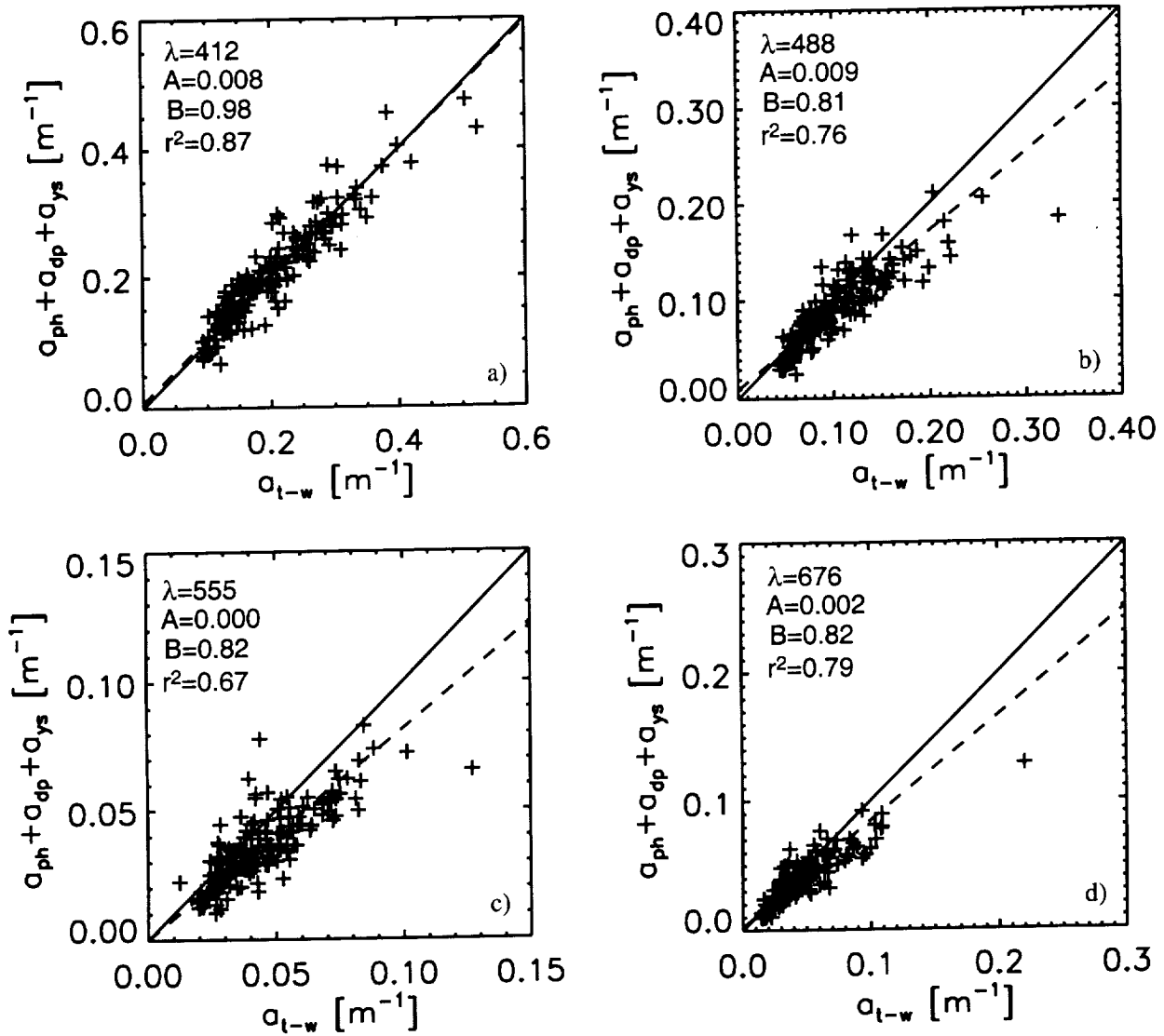† Milli-Q is a trademark of Millipore Corporation (Bedford, Massachusetts).

Fig. 4. Scatterplots of $a_{ph} + a_{dp} + a_{ys}$ from discrete seawater samples and a_{t-w} from AC-9 data computed by applying the scattering correction method 3 (using 177 samples at 1, 8, and 14 m). The dashed line (whose intercept A, slope B, and the determination coefficient r^2 are given in the panels) show the fitting line produced with the "robust" least absolute deviation method (Press et al. 1987). Plots are given for wavelengths of **a)** 412 nm, **b)** 488 nm, **c)** 555 nm, and **d)** 676 nm.

the clean-water calibrations performed in CoASTS during the 1995–1998 period, do not fully resolve short-term drifts in the instrument response.

8.5 Ancillary Field Data Measurements

Salinity $S_w(z)$ (in practical salinity units) and temperature $T_w(z)$ (in units of degrees Celsius) profiles are obtained at the same time as the WiSPER and AC-9 profiles (and are needed for AC-9 data processing). The tide level T_l and the Secchi depth SD were recorded for each station, together with major meteorological quantities taken at about 15 m above the sea surface: atmospheric pressure, P_a (in units of hectopascals); relative humidity, RH (in percent); air temperature, T_a (in degrees Celsius), wind speed, W_s (in meters per second); and wind direction, W_d (in true degrees). In addition, sea state, M [using the World Meteorological Organization (1983) code], and cloud cover, CC, observations in quarters are recorded to provide qualitative information for interpreting (apparently) spurious cases.

8.6 $a_p(\lambda)$ Measurements

The *in vivo* absorption coefficient, $a_p(\lambda)$, of aquatic particles retained on filters (in units per meter), is determined with a Perkin Elmer (Fremont, California) Lambda-19 dual-beam spectrometer equipped with a 60 mm diameter integrating sphere. The deposit of the particles on filters is obtained by filtration of seawater samples on glass

fiber (GF) filters with a nominal pore size of $0.7\,\mu m$ under low vacuum pressure (less than $120\,mm\,Hg$) to prevent particle breakage and pigment degradation. The filtered volume varies from $1.0-2.5\,L$, and is a function of the quantity of material suspended in the seawater. After filtration, the filters with the deposits are immediately placed on a Petri slide and stored in liquid nitrogen. The total absorption coefficient of the equivalent particle suspension in the 400–750 nm spectral range (with 1 nm resolution) is computed according to:

$$a_p(\lambda) = 2.3 A_{sus}(\lambda)\frac{F_a}{V_w}, \qquad (17)$$

where V_w is the volume of filtered water in liters, F_a is the filter clearance area in square centimeters, and $A_{sus}(\lambda)$ is the equivalent particle suspension absorbance obtained from the Transmission and Reflection (T-R) method proposed by Tassan and Ferrari (1995), which has been shown to be appropriate for the analysis of water samples characterized by highly backscattering mineral particles or by highly absorbing sediments.

Alternative to the T-R method, is the transmission method (T), which simply assumes that particle absorption is negligible in the near infrared and the effects of scattering are wavelength independent (Mitchell and Kiefer 1988). These simpler assumptions may be valid for oceanic water dominated by phytoplankton exhibiting no absorption in the near infrared, but are inadequate for coastal water containing large fractions of nonpigmented material (which may show an appreciable absorption in the near infrared, as well as wavelength-dependent scattering).

The two components of the particulate absorption coefficient for the pigmented and nonpigmented fractions, $a_{ph}(\lambda)$ and $a_{dp}(\lambda)$, respectively, are obtained through bleaching the sample on the filter using a solution of sodium hypochlorite (NaClO) as an oxidizing agent. This oxidation acts rapidly on pigment molecules and slowly on detritus making possible a selective analysis of the absorption components of pigmented and nonpigmented particles retained on the filter. A description of the NaClO bleaching technique, is presented in Tassan and Ferrari (1995) and in Ferrari and Tassan (1999).

Uncertainty in the estimate of the particle absorption coefficients is induced by the use of GF filters with a nominal $0.7\,\mu m$ pore size. In fact, these filters do not allow bacteria and the fraction of mineral particles with diameters lower than $0.7\,\mu m$ to be accounted for. In general, however, the absorption of these small mineral particles is negligible compared to the total absorption. The absorption of bacteria is almost 10 times lower than that of algal cells, and 5–10 times lower than that of cyanobacteria (Morel and Ahn 1990) characterized by a mean cell diameter of approximately $1\,\mu m$.

Figure 5 shows the scatterplots of $a_p(\lambda)$ obtained with the T method versus the T-R method at the representative wavelengths 412, 490, 555, and 665 nm. The $a_p(\lambda)$

data in Fig. 5 shows a good agreement at 555 nm with average percent differences of 5% displayed by the least-squares fit. The $a_p(\lambda)$ values obtained with the T method, however, show some overestimate with respect to the T-R method at wavelengths shorter than 510 nm (exhibiting average percent differences up to 11%) and some underestimate at longer wavelengths (exhibiting average percent differences up to -15% at 555 nm). The latter differences are due to the assumptions of $a_p(750) = 0$ and wavelength-independent of scattering in the T method). Pronounced differences can be observed (not shown here) between the $a_{ph}(\lambda)$ data obtained with the two methods applied to the bleached samples, while the $a_{ph}(\lambda)$ data from the T method only exhibit a slight general overestimate with respect to the T-R method. The dependence on wavelength of the regression fits given in the different scatterplots in Fig. 5 is a clear indication of the relevance of the spectral dependence of the scattering correction for the considered samples.

The repeatability and reproducibility of the CoASTS *in vivo* particulate absorption measurements were investigated using two types of analyses:

1) Duplicate analysis of the same samples (each filter sample was analyzed twice) for repeatability; and

2) Analysis of replicate samples (two separate samples obtained from the same water collection event were analyzed) for reproducibility.

Results from the two types of analyses are summarized in Table 6 at different wavelengths.

The duplicate analysis of the same samples, show average APDs varying from $3.0 \pm 2.6\%$ at 412 nm for $a_p(\lambda) = 0.084 \pm 0.044\,m^{-1}$, up to $7.4 \pm 6.0\%$ at 555 nm for $a_p(\lambda) = 0.023 \pm 0.011\,m^{-1}$. The former differences are attributed to instrument sensitivity, which can induce large uncertainties in the presence of samples characterized by weakly absorbing deposits on filters (e.g., because of the filtration of a small seawater volume). A second reason for the former differences could be a slight variation in the mechanical repositioning of the sample in front of the aperture of the integrating sphere, added to the spatial nonhomogeneity of the deposit on the filter. These combined effects may significantly change the sample area viewed by the spectrometer through the integrating sphere aperture of approximately $150\,mm^2$.

The analysis of replicate samples shows average APDs of $9.5 \pm 5.5\%$ at 412 nm for $a_p(\lambda) = 0.093 \pm 0.051\,m^{-1}$, and $9.8 \pm 7.0\%$ at 555 nm for $a_p(\lambda) = 0.024 \pm 0.012\,m^{-1}$. The former differences, increased by a few percent with respect to those given for the duplicate analysis of samples, are justified by

- The spatial nonhomogeneity of the deposits on the filters,
- Actual differences between samples, and
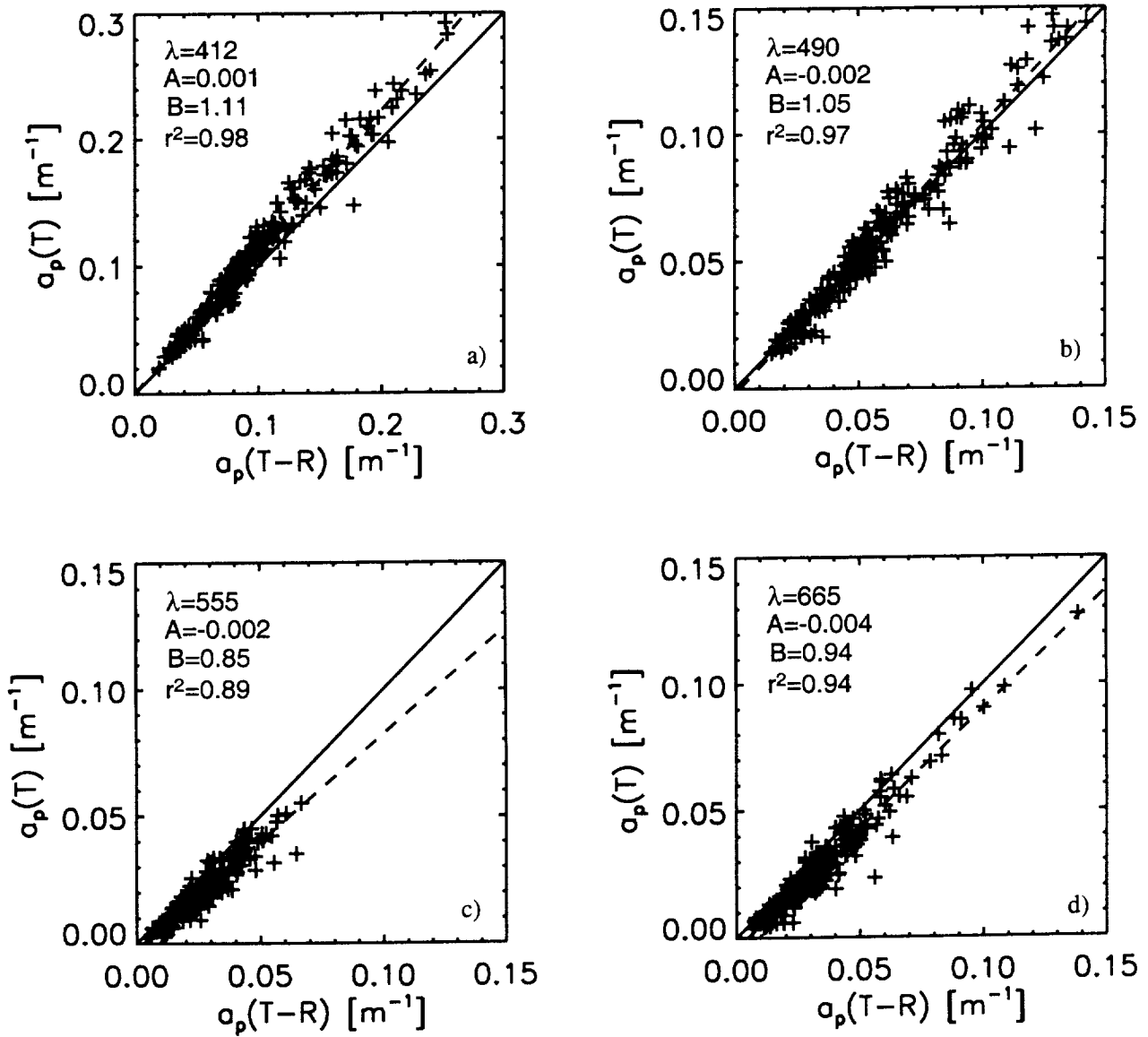- Instrument sensitivity.

Fig. 5. Scatterplots of a_p obtained with the T method versus the T-R method (using 332 surface samples). The dashed line indicates the least-squares fitting line (whose intercept A, slope B, and the determination coefficient r^2, are given in the panels). Plots are given for wavelengths of **a)** 412 nm, **b)** 490 nm, **c)** 555 nm, and **d)** 665 nm.

Table 6. Summary results on the analysis of $a_p(\lambda)$ measurements at different wavelengths (in nanometers). The average APDs resulting from duplicate analysis of the same sample is d_1. The average APDs resulting from analysis of replicate samples is d_2. The parentheses indicate the average $a_p(\lambda)$ values (in units of per meter) for the analyzed samples, and the standard deviations are indicated by the "$\pm$" sign.

λ [nm]	412	443	490	510	555	665
d_1 [%] $n = 21$	3.0 ± 2.6 (0.084 ± 0.044)	2.9 ± 2.3 (0.082 ± 0.042)	3.7 ± 2.7 (0.055 ± 0.026)	4.6 ± 3.3 (0.041 ± 0.019)	7.4 ± 6.0 (0.023 ± 0.011)	7.2 ± 5.8 (0.027 ± 0.015)
d_2 [%] $n = 21$	9.5 ± 5.5 (0.093 ± 0.051)	8.9 ± 5.9 (0.090 ± 0.049)	8.3 ± 5.4 (0.059 ± 0.030)	8.3 ± 5.2 (0.044 ± 0.021)	9.8 ± 7.0 (0.024 ± 0.012)	10.7 ± 7.6 (0.028 ± 0.017)

Table 7. A summary of the results on the analysis of $a_{ys}(\lambda)$ measurements at different wavelengths (in nanometers). The average APDs resulting from duplicate analysis of the same sample is d_1, and the average APDs resulting from the analysis of replicate samples (in this case, two replicates) is d_2. The parentheses indicate the average $a_{ys}(\lambda)$ values (in units of per meter) for the analyzed samples, and the standard deviations are indicated by the "$\pm$" sign.

λ [nm]	412	443	490	510	555
d_1 [%] $n = 21$	10.1 ± 7.3 (0.168 ± 0.037)	12.4 ± 8.4 (0.097 ± 0.022)	20.7 ± 15.0 (0.044 ± 0.011)	21.5 ± 15.7 (0.031 ± 0.007)	24.2 ± 19.8 (0.015 ± 0.005)
d_2 [%] $n = 21$	12.1 ± 6.3 (0.175 ± 0.038)	15.8 ± 8.8 (0.103 ± 0.026)	26.9 ± 17.5 (0.047 ± 0.015)	25.8 ± 18.0 (0.035 ± 0.011)	30.3 ± 23.8 (0.018 ± 0.005)

The study on reproducibility of $a_p(\lambda)$ also gives an estimate of the precision of the whole measurement procedure applied in CoASTS (including seawater sampling, filtration of samples, and spectrometric analysis). Focused studies on the accuracy of the T-R method are given in Tassan and Ferrari (1995 and 2002).

8.7 $a_{ys}(\lambda)$ Measurements

The absorption coefficient of CDOM or so-called *yellow substance*, $a_{ys}(\lambda)$ in units of per meter, is determined using a dual-beam spectrometer Perkin Elmer Lambda-12. Water samples (generally 0.7–1 L) are filtered through 0.22 μm cellulose filters and then refrigerated at 4°C in an amber glass bottle with the addition of a solution (0.5 mL for 100 mL of sample) of $10\,g\,L^{-1}$ of sodium azide (NaN_3) to prevent the growth of any bacteria. The spectrometric measurements, which are generally carried out within a few days, are performed in the spectral range 350–750 nm with 1 nm resolution. They are performed by placing a 10 cm quartz cuvette containing Milli-Q water in the optical path of the reference beam, and a 10 cm quartz cuvette containing the filtered seawater sample in the optical path of the sample beam. The spectral absorption coefficient $a_{ys}(\lambda)$ is computed from the measured absorbance $A_{ys}(\lambda)$ resulting from the difference between the sample absorbance and the reference absorbance (Ferrari et al. 1996):

$$a_{ys}(\lambda) = 2.3 \frac{A_{ys}(\lambda)}{L_c}, \qquad (18)$$

where $A_{ys}(\lambda)$ is the measured absorbance, and L_c is the pathlength (in meters) of the cuvette. The instrument background is removed using measurements obtained with Milli-Q water in both the sample and the reference cuvettes.

The use of 0.22 μm pore size filters to *define* CDOM, when 0.7 μm pore size filters are used for particle absorption, indicates the overall absorption budget cannot be fully resolved. In fact, bacteria, colloids, and very small mineral particles having sizes between 0.2–0.7 μm are not included in the absorption analysis. Their inclusion in the filtered seawater sample for $a_{ys}(\lambda)$ analysis, however,

would likely lead to an overestimate of the absorption coefficient because of their very high scattering and low absorbing properties (Stramsky and Mobley 1997, and Pak et al. 1971).

The repeatability and reproducibility of $a_{ys}(\lambda)$ measurements were investigated through duplicate analysis of the same samples and analysis of replicate samples, respectively. The analysis was carried out using $a_{ys}(\lambda)$ spectra corrected by the background signal at 600 nm [i.e., for each spectrum, $a_{ys}(600)$ is subtracted from $a_{ys}(\lambda)$ at all wavelengths assuming CDOM is not absorbing in the red domain]. The results of this analysis are summarized in Table 7 at different wavelengths.

The duplicate analysis of the same samples shows average APDs vary as a function of the absorption value from $10.1 \pm 7.3\%$ at 412 nm for $a_{ys}(\lambda) = 0.168 \pm 0.037\,m^{-1}$, up to $24.2 \pm 19.8\%$ at 555 nm for $a_{ys}(\lambda) = 0.015 \pm 0.005\,m^{-1}$. These differences are mostly attributed to temperature differences between the seawater sample and the reference Milli-Q water, the formation of microbubbles on the wall of the cuvettes, and mechanical alignment of the cuvettes.

The analysis of the replicate samples shows increased average APDs, when compared to the duplicate analysis, varying from $12.1 \pm 6.3\%$ at 412 nm for $a_{ys}(\lambda) = 0.175 \pm 0.038\,m^{-1}$ up to $30.3 \pm 23.8\%$ at 555 nm for $a_{ys}(\lambda) = 0.018 \pm 0.005\,m^{-1}$. The latter increase in differences, with respect to differences computed from duplicate analysis, are justified by differences between samples.

8.8 Pigment Measurements

Phytoplankton pigment concentrations are determined using HPLC analysis with a slightly modified Joint Global Ocean Flux Study protocol (JGOFS 1994 and Jeffrey et al. 1997). Seawater volumes, ranging from 1.0–2.5 L, set as a function of the quantity of material suspended in the seawater, are filtered immediately after collection using GF filters with a nominal pore size of 0.7 μm. The filters are then immediately stored in liquid nitrogen for subsequent laboratory analysis. Using the 0.7 μm pore size is justified by the diameter of living phytoplankton cells, which is generally higher than 1 μm (Stramsky and Kiefer 1991).

Pigment extraction is carried out in dim light by soaking each filter in 5 mL of a solution composed of 100%

G. Zibordi, J.-F. Berthon, J.P. Doyle, S. Grossi, D. van der Linde, C. Targa, and L. Alberotanza

acetone and $0.2\,\mu g\,L^{-1}$ canthaxanthin [used as an internal standard (IS)], and then grinding it with a Teflon® † pestle for 30 s at 0°C in a thermostatic tube. After storing the reworked sample for 24 h in a −18°C freezer, it is filtered in dim light using a syringe with a 0.45 μm GF filter and then taken to ambient temperature. Finally, 150 μL of a buffer solution composed of 0.5 M ammonium acetate (which ensures a better peak separation) is added to 500 μL of the filtrated extract and injected into the 200 μL HPLC loop. From the HPLC chromatogram, the concentration of each pigment, C_p ($\mu g\,L^{-1}$), is computed using

$$C_p = \frac{A_p f_p V_e}{V_i V_w B_e} \frac{A_r}{A_s}, \tag{19}$$

where A_p [in milli-Absorbance Units (AU) per second] is the pigment peak area; f_p is the relative response factor for each pigment; V_e (in milliliters) is the volume of the pigment extract; V_i (in microliters) is the volume injected into the HPLC; V_w (in liters) is the filtered volume; B_e is the buffer extract dilution factor (i.e., the ratio between the 500 μL of extract volume and the sum of the 500 μL of extract volume to the 150 μL of buffer solution); A_r (in milli-AU per second) is the reference IS peak area; and A_s (in milli-AU per second) is the sample IS peak area. The factor f_p (in units of $ng\,mAU^{-1}\,s^{-1}$) is specific for each pigment and is obtained through calibration of the instrument response with pigment standards. The reference IS peak area, A_r, is computed from the HPLC chromatogram of a reference solution of $0.2\,\mu g\,L^{-1}$ IS (A_r is recomputed at least once per day).

The use of an IS allows correction for uncertainties caused by evaporation or experimental losses during pigment extraction. System calibration is performed on an annual basis using pigment standards provided by the DHI Water and Environment Institute‡ (Høsholm, Denmark). The list of analyzed pigments are as follows:

- Chlorophyll a,
- Chlorophyll b,
- Chlorophylls c_1 and c_2,
- Chlorophyllide a,
- Fucoxanthin,
- Diadinoxanthin,
- β-carotene,
- Zeaxanthin,
- Alloxanthin,
- 19'-butanoyloxyfucoxanthin,
- 19'-hexanoyloxyfucoxanthin, and
- Diatoxanthin.

---

† Teflon is a registered trademark of E.I. du Pont de Nemours, Wilmington, Delaware.

‡ Formerly the VKI Water Quality Institute.

The scatterplot of total pigment concentration versus total chlorophyll a (chlorophyll a plus chlorophyllide a), is shown in Fig. 6 as an empirical quality assurance of the data. The results exhibit a high correlation (98% of the variance explained by the linear fit), and the slope of the linear fit (i.e., 2.05) is in close agreement with the value of 1.96 published by Aiken et al. (1995) for a data set including measurements from different oceanographic bio-optical provinces.
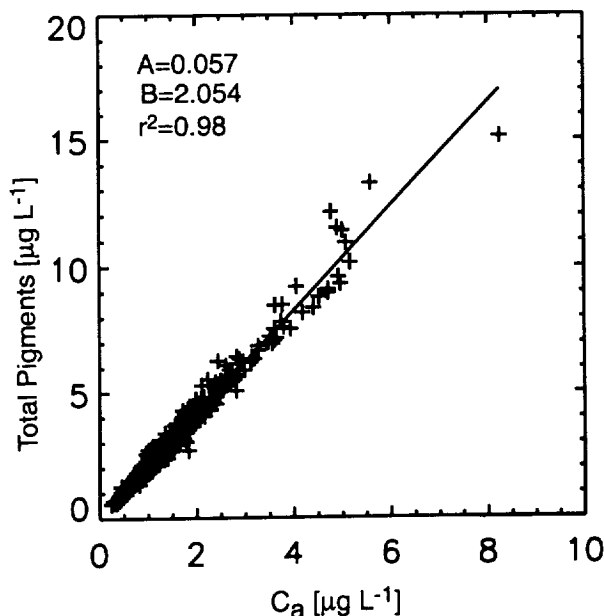

Fig. 6. A scatterplot of total pigments versus total chlorophyll a (C_a), defined as chlorophyll a plus chlorophyllide a (including intercept A, slope B, and the determination coefficient r^2).

In order to evaluate the precision of measurements performed with the described method, different experiments were carried out to estimate repeatability through duplicate analysis of the same samples and reproducibility using two methods:

a) Analysis of replicate samples, and

b) An intercomparison analysis of replicate samples by a different laboratory using a different measurement system and a different method.

Results from these experiments are summarized in Table 8 for some of the most represented pigments in the northern Adriatic Sea.

The duplicate HPLC analysis of samples shows average APDs in C_a of $1.4 \pm 1.2\%$ for 24 samples with an average concentration of $1.18 \pm 0.65\,\mu g\,L^{-1}$ (this variability can only be attributed to the sensitivity of the measurement system). The analysis of replicate samples, shows average absolute percentage differences in C_a of $7.1 \pm 6.3\%$ estimated using 36 pairs of samples with a mean concentration of $0.86 \pm 0.19\,\mu g\,L^{-1}$ (these differences are attributed

Table 8. A summary of the results on the analysis of HPLC data for the most represented pigments in the northern Adriatic Sea. The average APDs resulting from the duplicate analysis of the same sample is d_1. The average APDs resulting from the analysis of replicate samples is d_2. The average APDs from replicate sample analyses performed by JRC and by LOV is d_3. The values in parentheses indicate the average concentration of pigments (in units of microgram per liter) for the analyzed samples, and the standard deviations are indicated by the "$\pm$" sign.

Pigment	Chlorophyll a	Chlorophyll b	Chlorophyll $c_1 + c_2$	Fucoxanthin	19'-Hexanoyloxy-fucoxanthin
d_1 [%] $n = 24$	1.4 ± 1.2 (1.18 ± 0.65)	2.8 ± 3.0 (0.07 ± 0.05)	4.7 ± 5.7 (0.12 ± 0.10)	1.1 ± 1.5 (0.42 ± 0.30)	3.2 ± 3.1 (0.14 ± 0.11)
d_2 [%] $n = 336$	7.1 ± 6.3 (0.86 ± 0.19)	7.8 ± 6.9 (0.13 ± 0.10)	14.4 ± 10.8 (0.08 ± 0.03)	5.2 ± 4.1 (0.14 ± 0.12)	8.1 ± 7.1 (0.08 ± 0.04)
d_3 [%] $n = 15$	13.1 ± 7.0 (2.05 ± 0.97)	14.9 ± 16.7 (0.12 ± 0.07)	30.2 ± 8.8 (0.49 ± 0.33)	21.0 ± 8.8 (0.98 ± 0.63)	5.4 ± 13.1 (0.17 ± 0.13)

to the sensitivity of the measurement system, to the efficiency of the pigment extraction, and to differences between the duplicate samples).

The intercomparison experiment, which used sample analyses from a different laboratory, involved the LOV, and was carried out in September 1998. Pigments were extracted by applying the methods previously described. The analysis was performed with different systems and by applying different methods to replicate samples. The CoASTS (JRC) method was the same one as described above, and LOV used the method described in Vidussi et al. (1996). The results showed average APDs in C_a of $13.1 \pm 7.0\%$ estimated over 15 samples with a mean concentration of $2.05 \pm 0.97 \mu g\,L^{-1}$. These differences are attributed to the use of different HPLC methods, different sensitivities of the measurement systems, different calibration accuracies, and differences between the duplicate samples.

An estimate of reproducibility between different laboratories is given by the difference between the uncertainty associated with the analysis of the replicate samples (d_2) and the total uncertainty estimated from the laboratory intercomparison (d_3). This reproducibility estimate (about 6% for chlorophyll a) is very similar to the reproducibility achieved during a recent HPLC intercomparison (Hooker et al. 2000b) based on open ocean samples (on average about 5.5% for chlorophyll a).

8.9 C_{TSM} Measurements

TSM concentration is obtained from the net weight of the material collected on GF filters with a 0.7 μm pore size following a slightly modified version of the method proposed by Strickland and Parsons (1972). Volumes of seawater (generally from 1–2 L) are filtered through pre-washed, pre-ashed, and pre-weighed 0.7 μm nominal pore size GF filters.

After seawater filtration, the filter (specifically the filtration area and border) is washed with distilled water and

stored at $-18°C$ for subsequent laboratory analysis. Before final weighing, the filters are dried at 75°C for 1 h, and then temporarily stored in a desiccator. The concentration of TSM (in milligrams per liter) is calculated using:

$$C_{TSM} = \frac{W_t - W_f - \bar{w}_b}{V_w}, \quad (20)$$

where W_t is the weight in milligrams of the sample filter after filtration; W_f is the weight in milligrams of the filter before filtration; and $\bar{w}_b$ is a correction term (in milligrams) introduced to account for changes in the weight of the filter sample due to changes induced by environmental conditions and handling effects between the two weighing steps.

The term $\bar{w}_b$ is obtained from blank filters (i.e., GF filters completely conditioned for TSM analysis, not used for seawater filtration, but subjected to the same processes as the sample filters: transportation to the measurement site and back, storage in the freezer, and subsequent filter drying). It is computed from the difference between the average final weight of the blank filters and their original average weight.

The use of GF filters with a 0.7 μm nominal pore size for TSM analysis, can produce underestimates of C_{TSM}, because of the loss of particles with diameters less than 0.7 μm. The filter rinsing for salt removal, plus the filter conditioning before and after filtration before weighing, however, can induce uncertainties much larger than the mass percentage of particles with diameters less than 0.7 μm.

An analysis of measurement reproducibility performed with 93 pairs of duplicate samples shows average APDs equal to $13.9 \pm 13.4\%$ for $C_{TSM} = 0.86 \pm 0.40\,mg\,L^{-1}$. The largest differences (i.e., greater than 30%) between duplicate samples, have been observed with C_{TSM} lower than $0.5\,mg\,L^{-1}$ and are attributed to the intrinsic uncertainty in sample preparation (i.e., water sample nonhomogeneity and filter rinsing).

Table 9. A summary of the results on the analysis of PSD measurements at different diameter ranges, in micrometers, of particles. The average APDs resulting from duplicate analysis of the same sample is d_1. The values in parentheses indicate the average number of particles N_p per cubic centimeter in the given diameter range, for the analyzed samples. The standard deviations are indicated by the "±" sign.

Diameter Range	2–3	3–5	5–7	7–10
d_1 [%] $n = 230$	17.8 ± 18.8 $(20,332 \pm 12,678)$	9.6 ± 11.1 $(11,346 \pm 7,588)$	15.8 ± 14.4 $(3,280 \pm 2,692)$	25.8 ± 22.9 $(1,559 \pm 1,580)$

Table 10. Chlorophyll a concentration C_a, total suspended matter C_{TSM}, and colored dissolved organic matter absorption coefficient $a_{ys}(400)$ at 1, 8, and 14 m depth from seawater sample analyses for the stations presented as case studies in Figs. 7–9.

Station	Date	Depth [m]	C_a [μg L^{-1}]	C_{TSM} [mg L^{-1}]	a_{ys} [m^{-1}]
C390401	26 February 1998	1	4.89	2.33	0.162
C390401	26 February 1998	8	1.75	0.53	0.106
C390401	26 February 1998	14	1.51	0.80	0.130
C400401	10 March 1998	1	1.29	0.53	0.089
C400401	10 March 1998	8	1.28	0.73	0.106
C400401	10 March 1998	14	1.38	1.27	0.097
C490201	9 September 1998	1	0.53	0.27	0.075
C490201	9 September 1998	8	0.51	0.27	0.013
C490201	9 September 1998	14	0.91	0.80	0.049

8.10 Particle Size Distributions

The rationale for making PSD measurements is a desire to support theoretical estimates of the seawater particle scattering phase function through Mie calculations. The PSD (i.e., the number and size of particles suspended in seawater) is measured using the Coulter Counter technique and making use of a MULTISIZER II† system. The Coulter Counter technique is based on the principle that particles, suspended in an electrically conductive liquid and forced to flow through a small aperture (orifice) having an immersed electrode on each side, change the resistance between the electrodes. The latter produces a voltage pulse proportional to the particle size, which can be detected and measured.

Analysis of seawater samples was carried out using a 100 μm aperture, which ensures characterization of particles in the diameter range of 1.8–64 μm distributed over 256 logarithmically spaced channels (i.e., the diameter associated with each channel halves every 50 channels down). For each sample, three sequential measurements are carried out with 2 mL of seawater each time and the resulting distribution is averaged. The background of particle size distribution is estimated making use of seawater filtered at 0.22 μm.

Absolute calibration of the MULTISIZER II system is performed annually making use of 5 μm monosized smooth particles (i.e., latex formulations of polystyrene divinyl benzene) of known density. Measurement repeatability was evaluated through duplicate analysis of samples from the

same water volume. The PSD results are given in Table 9 for different ranges of particle diameters (i.e., 2–3, 3–5, 5–7, and 7–10 μm), and show average APDs ranging from 9.6–25.8% in the 3–5 μm and 7–10 μm ranges, respectively. The larger average differences observed in the 2–3 μm interval, when compared to the 3–5 μm interval, are due to an increase in the measurement noise at the lower limit of the measurement interval, i.e., 1.8 μm.

9. SAMPLE DATA

A comprehensive and detailed analysis of the data collected in the framework of the CoASTS Project for a three-year period starting in the latter part of 1995 is given in Berthon et al. (2002). For completeness of the overall work, an overview of optical and hydrographic profiles typical of the AAOT site in the northern Adriatic Sea is given here and discussed below.

In Figs. 7–9, $\hat{L}_u(z, \lambda)$ and $c_{t-w}(z, \lambda)$ at representative wavelengths plus $S_w(z)$ are displayed for three different stations: C390401 on 26 February 1998, C400401 on 10 March 1998, and C490201 on 9 September 1998. Relevant variables identifying the seawater biogeochemical and optical characteristics of the stations are given in Table 10.

Figure 7 displays the profiles for station C390401 and shows some seawater vertical stratification between the surface and 3 m depth. Coefficients of $c_{t-w}(z, \lambda)$ show a sharp variation of about a factor of four at 412 nm, in a few meters range around 3 m depth. In agreement with these changes, $\hat{L}_u(z, \lambda)$ profile data (in logarithmic scale) show a change in slope at the same depth. The seawater salinity
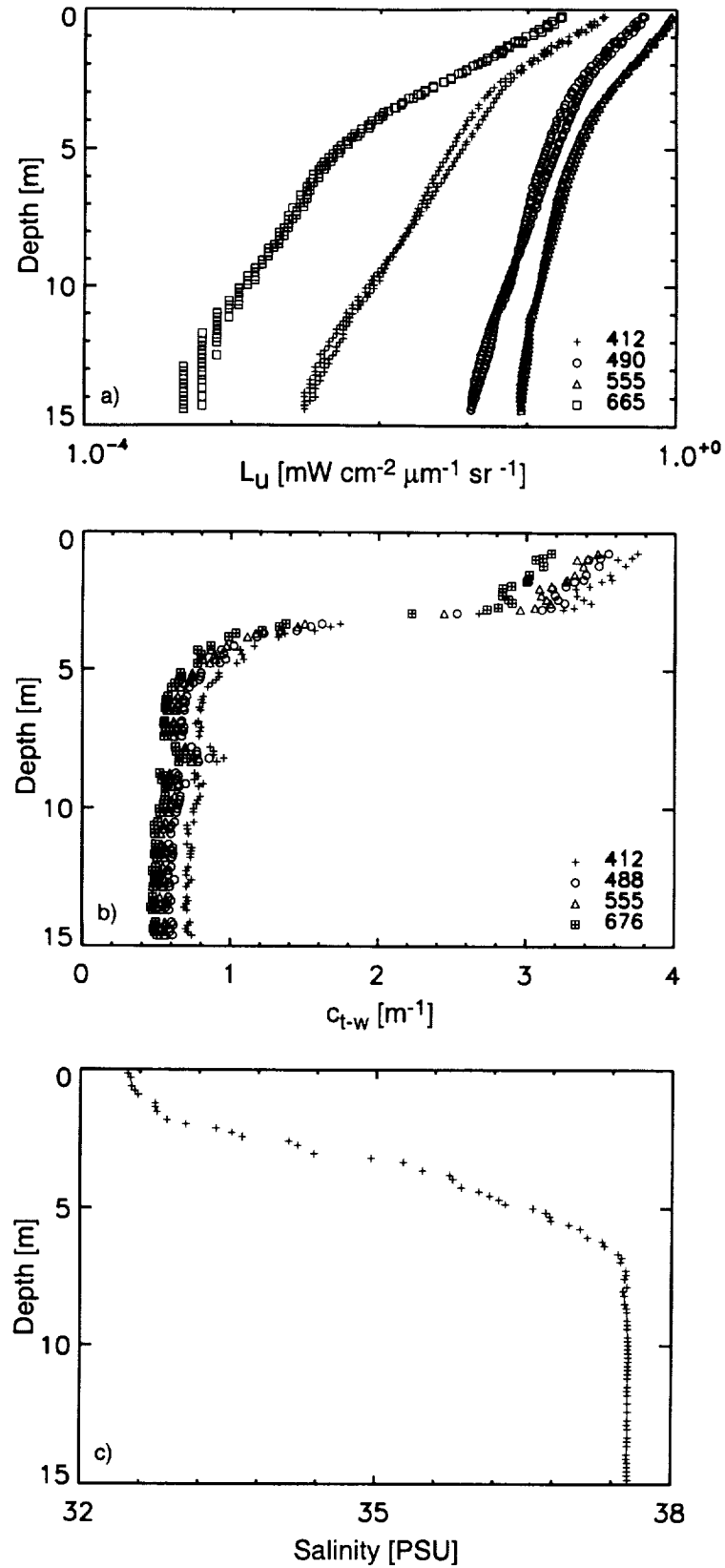
† Manufactured by Beckman Coulter, Inc., Hialeah, Florida.

Fig. 7. Profiles of $\hat{L}_u(z, \lambda)$, $c_{t-w}(z, \lambda)$, and $S_w(z)$ in panels **a)**, **b)**, and **c)**, respectively, for station C390401 on 26 February 1998 (the irregular distribution of $c_{t-w}(z, \lambda)$ data with respect to depth, is due to the loss of data over the serial link).
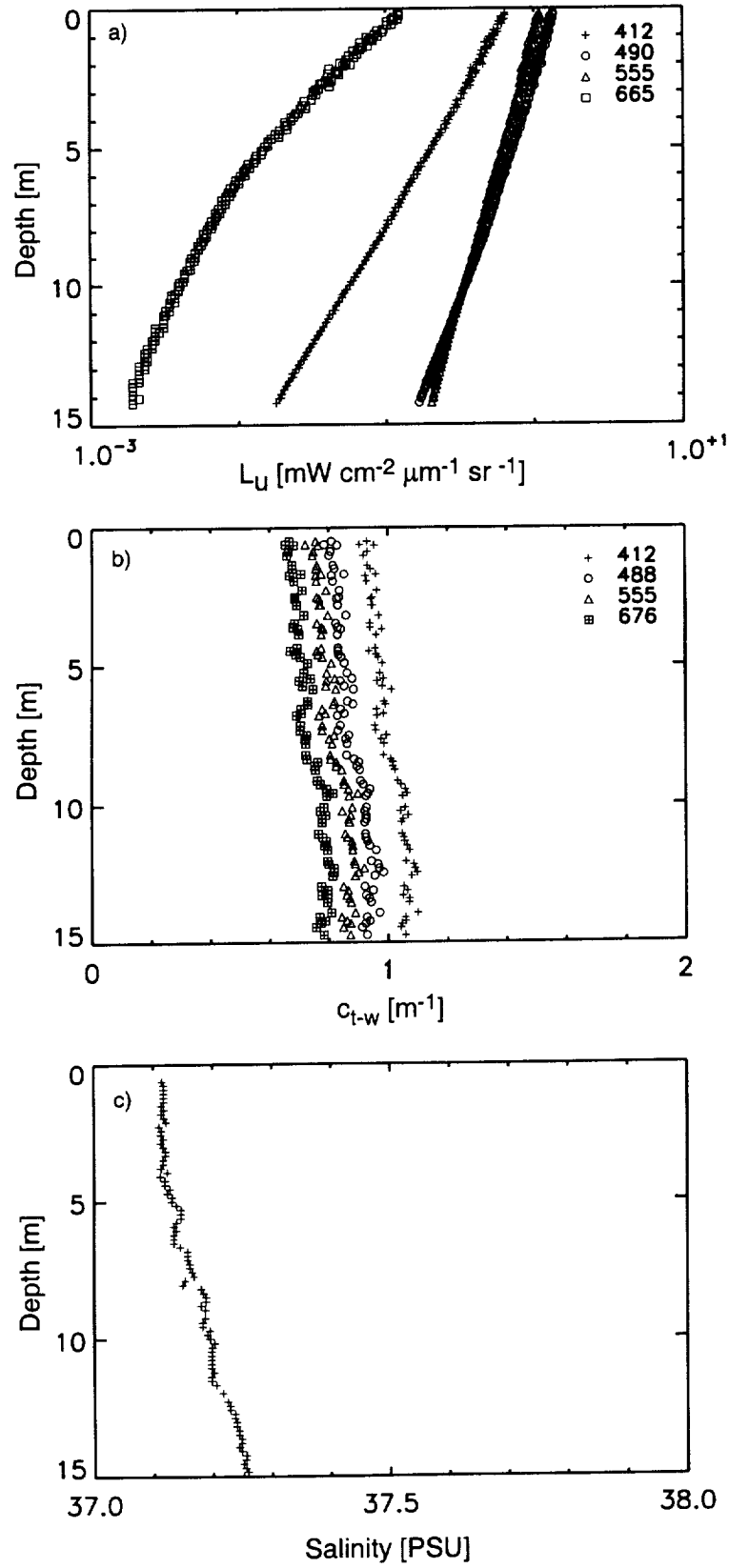
G. Zibordi, J.-F. Berthon, J.P. Doyle, S. Grossi, D. van der Linde, C. Targa, and L. Alberotanza

Fig. 8. As in Fig. 7, but for station C400401 on 10 March 1998.
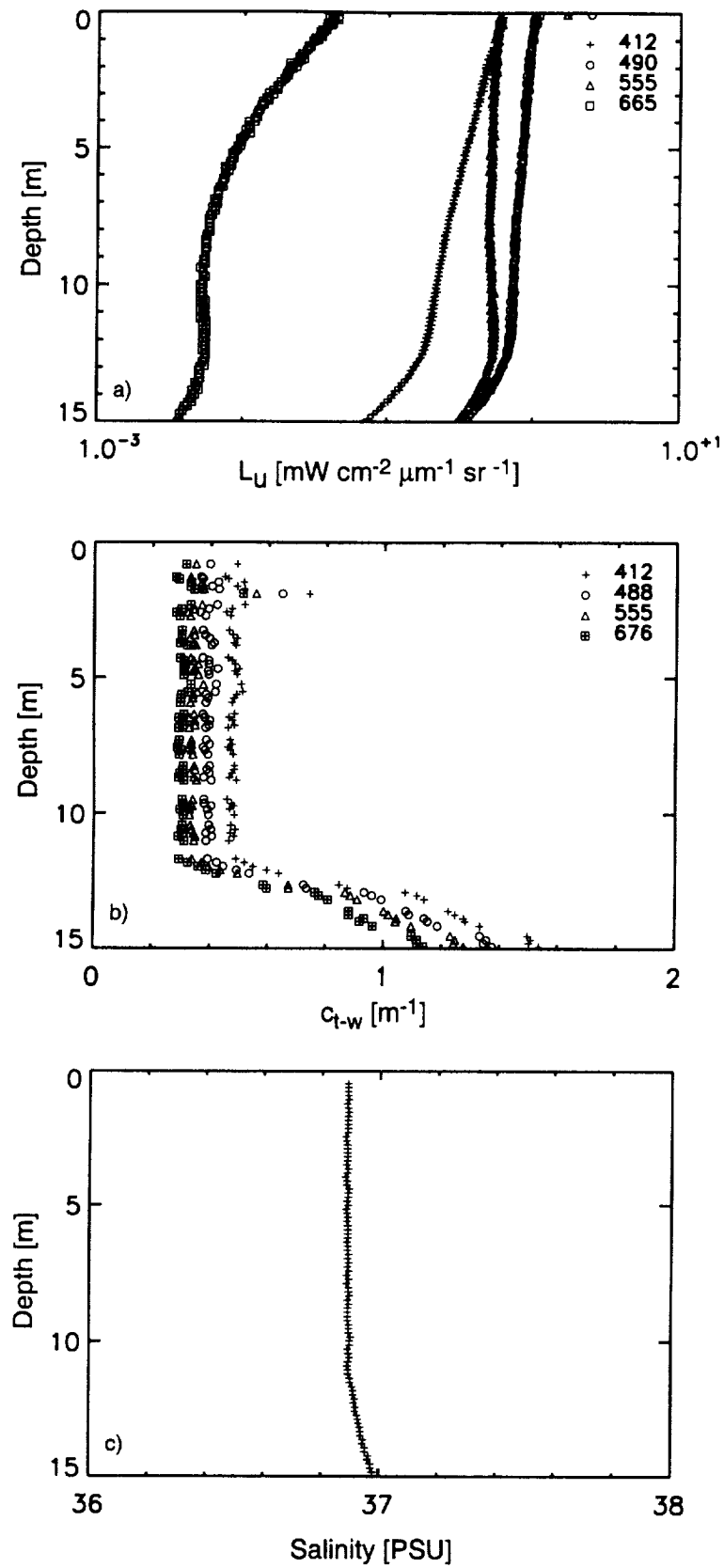
Fig. 9. As in Fig. 7, but for station C490201 on 9 September 1998.

exhibits a layer with approximately 33 PSU between the surface and 2 m depth, followed by an abrupt increase up to 37 PSU from 2–6 m. This profile can be explained by the existence of a layer of fresh water, rich in particles and CDOM originating from the major northern rivers that drain into the northern Adriatic Sea. The relatively high values of C_a, C_{TSM}, and to a lesser extent of a_{ys} in the surface layer (i.e., 1 m depth), given in Table 10 for station C390401, clearly support this hypothesis. In addition, the high concentration of C_a (i.e., 4.89 μg L^{-1}) in the same surface layer, suggests the presence of nutrients is probably due to coastal transport.

Figure 8 presents the profiles for station C400401, for which the water column is vertically unstratified. Both the $c_{t-w}(z, \lambda)$ and $S_w(z)$ values show very slight changes as a function of depth. In full agreement with this, $\ln \left[\hat{L}_u(z, \lambda) \right]$ (excluding the data at 665 nm) exhibits a linear decay as a function of depth with no significant change in slope. With the exception of C_{TSM}, which shows some slight increase with depth, the C_a and a_{ys} data for station C400401 (Table 10) do not exhibit any relevant change with depth, which is in complete agreement with the profiles presented in Fig. 8.

Figure 9 displays the profiles for station C490201 and shows a stratification near the bottom. The $c_{t-w}(z, \lambda)$ data displays almost constant values from the surface up to 12 m depth, and then exhibits a sharp increase by a factor of about 3 from 12–15 m depth. This feature is confirmed by a change in the slope of $\hat{L}_u(z, \lambda)$ at 12 m depth. An explanation for this could be the existence of a bottom current or vertical mixing, because the water is almost homogeneous in $S_w(z)$, thereby resuspending the particles. The former observations are supported by the C_{TSM} data at 14 m depth, which exhibit values three times higher than those at 1 and 8 m.

The sample data presented here, although far from describing all the possible conditions encountered at the AAOT site, give a general overview of the variability that can characterize a coastal measurement site in the northern Adriatic Sea.

10. CONCLUSIONS

This report presented the measurement program used within the CoASTS Project (at the AAOT site) and extensively discussed the applied methods with a particular emphasis on those more relevant for bio-optical modeling and the calibration and validation of ocean color sensors. The methods discussed for the analysis of radiometric measurements highlighted the importance of correcting in-water radiance and irradiance data from superstructure (tower-shading) effects, instrument self-shading, and bottom effects. These perturbations for the specific measurement conditions analyzed in this study, may induce an overall spectral uncertainty in $L_u(0^-\lambda)$ ranging from 4–18% at 412 nm, −2 to +10% at 490 nm, −9 to +10% at 555 nm, and 6–16% at 665 nm.

The intercomparison of seawater absorption coefficients from AC-9 in situ measurements and from laboratory spectrometric analysis of discrete seawater samples, showed the best agreement when the scattering correction—for perturbation effects induced in AC-9 data by the finite acceptance angle of the optics and the non-ideal reflective surface of the absorption chamber—is performed removing a variable percentage of the scattering coefficient. In this case, the scatterplots of the absorption coefficients from spectrometric analysis of seawater samples and AC-9 measurements showed average absolute percentage differences of −2, −19, −18, and −18% at 412, 488, 555, and 676 nm, respectively.

The intercomparison of the spectrometric transmission method with the T-R method used in CoASTS for the analysis of seawater particulate absorption $a_p(\lambda)$, showed differences ranging from +11% up to −15% in the 412–665 nm spectral interval. The reproducibility of CoASTS particulate and yellow substance absorption coefficients, determined with an analysis of replicate samples, showed average APDs of 9.5 ± 5.5% for $a_p(412) = 0.093 \pm 0.051$ m^{-1} and 12.1 ± 6.3% for $a_{ys}(412) = 0.175 \pm 0.038$ m^{-1}, respectively.

A measurement reproducibility study, using replicate samples, was also presented in determining the concentration of the most represented pigments in the northern Adriatic Sea obtained with HPLC analysis. The results for C_a showed average APDs of 7.1 ± 6.3% for $C_a = 0.86 \pm 0.19$ μg L^{-1}. A similar analysis was carried out to assess the reproducibility of C_{TSM} measurements. The latter results showed average APDs of 13.9 ± 13.4% for $C_{TSM} = 0.86 \pm 0.40$ mg L^{-1}, exhibiting the largest differences (i.e., up to 30%) for concentrations lower than 0.5 mg L^{-1}.

The study on measurement reproducibility highlighted a strong variability for all quantities obtained from the analysis of replicate samples produced from the same volume of seawater, and suggested difficulties in properly homogenizing the water volume during the preparation of the samples.

The uncertainty, repeatability, and reproducibility analyses presented in this study, were a first attempt to estimate the accuracies in the different quantities measured within the CoASTS Project. Although some of the results may suggest an unsatisfactory accuracy for specific applications, it must be remembered that the coastal nature of the study area significantly increases the measurement difficulties, and in many cases, may reduce the achievable accuracies.

The sample profile data, gave an overview of the typical seawater bio-optical characteristics at the measurement site. Their variability, assumed to be quite representative of the whole northern Adriatic Sea, confirms the possibility of exploring very different water types at a single measurement point and, thus, sustains the suitability of the AAOT measurements to support bio-optical modeling, as well as calibration and validation activities for northern Adriatic Sea coastal waters.

GLOSSARY

AAOT — *Acqua Alta* Oceanographic Tower
A/D — Analog-to-Digital
ADEOS — Advanced Earth Observing Satellite
AERONET — Aerosol Robotic Network
APD — Absolute Percent Difference
ARGOS — Not an acronym, but the name given to the data collection and location system on the NOAA operational satellites.
BOUSSOLE — *Bouée pour l'acquisition de Séries Optiques à Long Terme* (buoy for the acquisition of a long-term optical series).
CDOM — Colored Dissolved Organic Matter
CNR — *Consiglio Nazionale delle Ricerche* (Italy)
CTD — Conductivity, Temperature, and Depth
CoASTS — Coastal Atmosphere and Sea Time Series
CZCS — Coastal Zone Color Scanner
DCP — Data Collection Platform
DHI — DHI Water and Environment Institute (Denmark)
FEL — Not an acronym, but a lamp designator.
GF — Glass Fiber Filter
GSFC — Goddard Space Flight Center
HPLC — High Performance Liquid Chromatography
IS — Internal Standard
ISDGM — *Istituto per lo Studio della Dinamica delle Grandi Masse* (Italy)
JGOFS — Joint Global Ocean Flux Study
JRC — Joint Research Centre (Italy)
LOV — *Laboratoire d'Océanographie de Villefranche* (France)
LPCM — *Laboratoire de Physique et Chimie Marines* (France)
LUT — Look-Up Table
MERIS — Medium Resolution Imaging Spectrometer
METEOSAT — Meteorological Satellite
MOBY — Marine Optical Buoy

MODIS — Moderate Resolution Imaging Spectroradiometer
MOS — Modular Opto-electronic Sensor
MVDS — Multichannel Visible Detector System
NASA — National Aeronautics and Space Administration
NASDA — National Space Development Agency (Japan)
NIST — National Institute of Standards and Technology
NOAA — National Oceanographic and Atmospheric Administration
OCI — Ocean Color Irradiance
OCR — Ocean Color Radiance
OCTS — Ocean Color and Temperature Scanner
PlyMBODy — Plymouth Marine Bio-Optical Data Buoy
PML — Plymouth Marine Laboratory (England)
POLDER — Polarization and Directionality of the Earth's Reflectance
PSD — Particle Size Distribution
SeaWiFS — Sea-viewing Wide Field-of-view Sensor
SNR — Signal-to-Noise Ratio
T — Transmission method for spectrophotometric analysis.
T-R — Transmission-Reflection (method for spectrophotometric analysis)
TSM — Total Suspended Matter
VKI — VKI Institute for Water Environment (Denmark)
WETLabs — Western Environmental Technology Laboratories (Inc.)
WiSPER — Wire-Stabilized Profiling Environmental Radiometer
YBOM — Yamato Bank Optical Mooring (Japan)
YES — Yankee Environmental Systems (Inc.)

SYMBOLS

$\hat{}$ — Indication of a measured quantity with any given variable.
$a(z, \lambda)$ — Total seawater absorption coefficient at depth z.
$a_{dp}(\lambda)$ — Nonpigmented particulate matter absorption coefficient.
$a_{dp}(z, \lambda)$ — Nonpigmented particulate matter absorption coefficient at depth z.
$a_p(\lambda)$ — Particulate matter absorption coefficient.
$a_p(z, \lambda)$ — Particulate matter absorption coefficient at depth z.
$a_{ph}(\lambda)$ — Pigmented particulate matter absorption coefficient.
$a_{ph}(z, \lambda)$ — Pigmented particulate matter absorption coefficient at depth z.
$a_{t-w}(z, \lambda)$ — $a_{t-w}^{ST}(z, \lambda)$ corrected for AC-9 scattering effects.
$\hat{a}_{t-w}(z, \lambda)$ — Total seawater minus pure seawater absorption coefficient from AC-9.
$\hat{a}_{t-w}^{ST}(z, \lambda)$ — $\hat{a}_{t-w}^{ST}(z, \lambda)$ corrected for salinity and temperature effects.
$a_{ys}(\lambda)$ — Colored dissolved organic matter absorption coefficient.
$a_{ys}(z, \lambda)$ — Colored dissolved organic matter absorption coefficient at depth z.

$a_w(\lambda)$ Pure seawater beam absorption coefficient.

av Average.

A Intercept.

A_p Pigment peak area.

A_r Reference internal standard peak area.

A_s Sample internal standard peak area.

$A_{sus}(\lambda)$ Equivalent particle suspension absorbance.

$A_{ys}(\lambda)$ Dissolved matter absorbance.

$b(\lambda)$ Total seawater scattering coefficient.

$b_{t-w}(z,\lambda)$ Total minus pure seawater scattering coefficient.

B Slope.

B_e Buffer-extract dilution factor.

$c(z,\lambda)$ Total seawater beam attenuation coefficient.

$c_{t-w}(z,\lambda)$ Total seawater minus pure seawater beam attenuation coefficient.

$\hat{c}_{t-w}(z,\lambda)$ Total seawater minus pure seawater beam attenuation coefficient from AC-9.

$\hat{c}_{t-w}^{ST}(z,\lambda)$ $\hat{c}_{t-w}(z,\lambda)$ corrected for salinity and temperature effects.

$c_w(\lambda)$ Pure seawater beam attenuation coefficient.

C_a Chlorophyll a concentration.

$C_{\hat{E}_d}(\lambda)$ Absolute calibration coefficient for $\hat{E}_d(z,\lambda)$.

$C_{\hat{E}_u}(\lambda)$ Absolute calibration coefficient for $\hat{E}_u(z,\lambda)$.

$C_{\hat{L}_u}(\lambda)$ Absolute calibration coefficient for $\hat{L}_u(z,\lambda)$.

C_p Pigment concentration.

$C_{\hat{\mathfrak{J}}}(\lambda)$ Absolute calibration coefficient for $\hat{\mathfrak{J}}(z,\lambda)$.

C_{TSM} The concentration of total suspended matter.

CC Cloud cover.

d_1 Average differences from duplicate analysis of the same sample.

d_2 Average differences from analysis of duplicate samples.

d_3 Average differences from duplicate samples analyzed by different laboratories.

$\bar{D}_{\hat{\mathfrak{J}}}(\lambda)$ Average dark value for $V_{\mathfrak{J}}(z,\lambda)$.

D_y Sequential day of the year.

$E(\lambda)$ Direct sun irradiance.

$E_0(\lambda)$ Extra-atmospheric sun irradiance.

$E_d(z,\lambda)$ Downward irradiance at depth z.

$\hat{E}_d(z,\lambda)$ $E_d(z,\lambda)$ affected by measurement perturbations.

$E_d(0^-,\lambda)$ Subsurface downward irradiance.

$E_d(0^+,\lambda)$ Above-water downward irradiance.

$\hat{E}_d(0^-,\lambda)$ $E_d(0^-,\lambda)$ affected by measurement perturbations.

$E_i(0^+,\lambda)$ Above-water downward diffuse irradiance.

$E_s(\lambda)$ Direct normal sun irradiance.

$E_u(z,\lambda)$ Upward irradiance at depth z.

$\hat{E}_u(z,\lambda)$ $E_u(z,\lambda)$ affected by measurements perturbation.

$E_u(0^-,\lambda)$ Subsurface upward irradiance.

$\hat{E}_u(0^-,\lambda)$ $E_u(0^-,\lambda)$ affected by measurement perturbations.

$E_u^{BC}(0^-,\lambda)$ Bottom corrected upwelling irradiance.

f_p Pigment specific calibration factor.

F_a Filter clearance area.

$I_{\hat{\mathfrak{J}}}(\lambda)$ Immersion coefficient.

$\hat{\mathfrak{J}}(z,\lambda)$ Absolute calibration of the considered radiometric quantities.

$\mathfrak{J}(0^-,\lambda)$ Subsurface radiometric quantity.

$\hat{\mathfrak{J}}(0^-,\lambda)$ Subsurface radiometric quantity affected by measurement perturbations.

$\hat{\mathfrak{J}}(0,\lambda)$ Radiometric quantity affected by measurement perturbations.

$k(z_B,\lambda)$ Transmittance for the downward plus upward normal optical paths between the surface and the bottom at depth z.

$K_{E_d}(\lambda)$ Diffuse attenuation coefficient from $E_d(z,\lambda)$.

$K_{\hat{E}_d}(\lambda)$ Diffuse attenuation coefficient from $\hat{E}_d(z,\lambda)$.

$\bar{K}_{E_d}(\lambda)$ Average profile diffuse attenuation coefficient from $E_d(z,\lambda)$.

$K_{\hat{E}_u}(\lambda)$ Diffuse attenuation coefficient from $\hat{E}_u(z,\lambda)$.

$K_{\hat{\mathfrak{J}}}(\lambda)$ Diffuse attenuation coefficient from $\hat{\mathfrak{J}}(z,\lambda)$.

$K_{\hat{L}_u}(\lambda)$ Diffuse attenuation coefficient from $\hat{L}_u(z,\lambda)$.

L_c Cuvette pathlength.

$L_i(\theta,\phi,\lambda)$ Diffuse sky radiance.

$L_u(z,\lambda)$ Upwelled radiance at depth z.

$\hat{L}_u(z,\lambda)$ $L_u(z,\lambda)$ affected by measurement perturbations.

$L_u(0^-,\lambda)$ Subsurface upwelled radiance.

$\hat{L}_u(0^-,\lambda)$ $L_u(0^-,\lambda)$ affected by measurement perturbations.

$L_u(0^+,\lambda)$ Above-water upwelled radiance.

$L_u^{BC}(0^-,\lambda)$ Bottom corrected upwelled radiance.

$L_{WN}(\lambda)$ Normalized water-leaving radiance.

m The relative air mass.

M Sea state.

n Number of points.

N Number of optical stations.

N_p Number of particles.

P_a Atmospheric pressure.

$Q_n(z,\lambda)$ $E_u(z,\lambda)/L_u(z,\lambda)$, i.e., the Q-factor at nadir.

$Q_n(0^-,\lambda)$ $E_u(0^-,\lambda)/L_u(0^-,\lambda)$.

$\hat{Q}_n(0^-,\lambda)$ $\hat{E}_u(0^-,\lambda)/\hat{L}_u(0^-,\lambda)$.

$r^2(\lambda)$ Determination coefficient.

$r_i(\lambda)$ Ratio between diffuse and direct above-water downward irradiance.

$R(z,\lambda)$ Bottom correction of irradiance reflectance.

$\hat{R}(0^-,\lambda)$ $\hat{E}_u(0^-,\lambda)/\hat{E}_d(0^-,\lambda)$.

R_I Instrument case radius.

R_S Sensor entrance optics radius.

RH Relative humidity.

$S_w(z)$ Seawater salinity at depth z.

SD Secchi disk depth.

T_a Air temperature.

T_l Tide level.

$T_w(z)$ Water temperature at depth z.

V_e Volume of pigment extract.

V_i HPLC injected volume.

$V_{\hat{\mathfrak{J}}}(z,\lambda)$ The $\hat{\mathfrak{J}}(z,\lambda)$ voltage (in digital counts).

V_w Volume of filtered water.

$\bar{w}_b$ Correction term.

W_d Wind direction.

W_f Filter weight before filtration.

W_s Wind speed.

W_t Filter weight after seawater filtration.

z Depth.

z_B Bottom depth.

z_0 Upper limit of the extrapolation depth.

z_1 Lower limit of the extrapolation depth.

δ Fixed percentage.

$\eta_{\hat{\jmath}}(\lambda)$ Perturbation correction factor for $\hat{\jmath}(0^-, \lambda)$.

$\eta_{\hat{\jmath}}^{BE}(\lambda)$ Bottom effects correction factor for $\hat{\jmath}(0^-, \lambda)$.

$\eta_{\hat{\jmath}}^{SS}(\lambda)$ Self-shading correction factor for $\hat{\jmath}(0^-, \lambda)$.

$\eta_{\hat{\jmath}}^{TS}(\lambda)$ Tower-shading correction factor for $\hat{\jmath}(0^-, \lambda)$.

θ Zenith angle.

θ_0 Sun zenith angle.

λ Wavelength.

λ_0 Reference wavelength.

$\rho_B(\lambda)$ Bottom reflectance.

σ Standard deviation.

τ Atmospheric optical thickness.

$\tau_a(\lambda)$ Aerosol optical thickness.

$\tau_o(\lambda)$ Ozone optical thickness.

$\tau_R(\lambda)$ Rayleigh (molecular) optical thickness.

ϕ Azimuth angle.

ϕ_0 Solar azimuth angle.

$\omega_0(\lambda)$ Single scattering albedo.

REFERENCES

Aiken, J., G.F. Moore, C. Trees, S.B. Hooker, and D. Clark, 1995: The SeaWiFS CZCS-Type pigment algorithm. *NASA Tech. Memo. 104566, Vol. 29,* S.B. Hooker and E.R. Firestone, Eds., NASA Goddard Space Flight Center, Greenbelt, Maryland, 34 pp.

Antoine, D., and P. Guevel, 2000: Calibration and validation of satellite ocean color observations: The BOUSSOLE Project. *Proc. Ocean Optics XV,* Monaco, October 16–20, 2000. [Available on CD-ROM: Office of Naval Research, Washington, DC].

Berthon, J.F., G. Zibordi, and S.B. Hooker, 2000: Marine optical measurements of a mucilage event in the northern Adriatic Sea, *Limnol. Oceanogr.,* **45,** 322–327.

——, G. Zibordi, J.P. Doyle, S. Grossi, D. van der Linde, and C. Targa, 2002: Coastal Atmosphere and Sea Time Series (CoASTS), Part 2: Data Analysis. *NASA Tech. Memo. 2002-206892, Vol. 20,* S.B. Hooker and E.R. Firestone, Eds., NASA Goddard Space Flight Center, Greenbelt, Maryland, 25 pp.

Clark, D.K., H.R. Gordon, K.J. Voss, Y. Ge, W. Broenkow, and C. Trees, 1997: Validation of atmospheric correction over the oceans, *J. Geophys. Res.,* **102,** 17,209–17,217.

D'Alimonte, D., G. Zibordi, and J-F. Berthon, 2001: "The JRC data processing system." In: Hooker, S.B., G. Zibordi J-F. Berthon, D. D'Alimonte, S. Maritorena, S. McLean, and J. Sildam, Results of the Second SeaWiFS Data Analysis Round Robin, March 2000 (DARR-00). *NASA Tech. Memo. 2001-206892, Vol. 15,* S.B. Hooker and E.R. Firestone, Eds., NASA Goddard Space Flight Center, Greenbelt, Maryland, 71 pp.

Doyle, J.P., and G. Zibordi, 2002: Monte Carlo modeling of optical transmission within 3-D shadowed field: Application to large deployment structures, *Appl. Opt.,* (in press).

Ferrari, G.M., M.D. Dowell, S. Grossi, and C. Targa, 1996: Relationship between the optical properties of chromophoric dissolved organic matter and total concentration of dissolved organic carbon in the southern Baltic Sea region, *Mar. Chem.,* **55,** 299–316.

——, and ——, 1999: A method for removal of light-absorption by phytoplankton pigments using chemical oxidation, *J. Phycol.,* **35,** 1,090–1,098.

Gordon, H.R., and K. Ding, 1992: Self-shading of in-water optical instruments, *Limnol. Oceanogr.,* **37,** 491–500.

Harrison, L., J. Michalsky, and J. Berndt, 1994: Automatic multifilter rotating shadow band radiometer: an instrument for optical depth and radiation measurements, *Appl. Opt.,* **33,** 5,118–5,125.

Holben, B.N., T.F. Eck, I. Slutsker, D. Tanre, J.P. Buis, A. Setzer, E. Vermote, J.A. Reagan, Y.J. Kaufman, T. Nakajima, F. Lavenu, I. Jankowiak, and A. Smirnov, 1998: AERONET—A federated instrument network and data archive for aerosol characterization, *Remote Sens. Environ.,* **66,** 1–16.

Hooker, S.B., G. Zibordi, G. Lazin, and S. McLean, 1999: The SeaBOARR-98 Field Campaign. *NASA Tech. Memo. 1999-206892, Vol. 3,* S.B. Hooker and E.R. Firestone, Eds., NASA Goddard Space Flight Center, Greenbelt, Maryland, 40 pp.

——, ——, J-F. Berthon, S.W. Bailey, and C.M. Pietras, 2000a: The SeaWiFS Photometer Revision for Incident Surface Measurement (SeaPRISM) Field Commissioning. *NASA Tech. Memo. 2000-206892, Vol. 13,* S.B. Hooker and E.R. Firestone, Eds., NASA Goddard Space Flight Center, Greenbelt, Maryland, 24 pp.

——, H. Claustre, J. Ras, L. Van Heukelem, J-F. Berthon, C. Targa, D. van der Linde, R. Barlow, and H. Sessions, 2000b: The First SeaWiFS HPLC Analysis Round-Robin Experiment (SeaHARRE-1). *NASA Tech. Memo. 2000-206892, Vol. 14,* S.B. Hooker and E.R. Firestone, Eds., NASA Goddard Space Flight Center, Greenbelt, Maryland, 42 pp.

——, S. McLean, J. Sherman, M. Small, G. Lazin, G. Zibordi, and J.W. Brown, 2002: The Seventh SeaWiFS Intercalibration Round-Robin Experiment (SIRREX-7), March 1999. *NASA Tech. Memo. 2002-206892, Vol. 17,* S.B. Hooker and E.R. Firestone, Eds., NASA Goddard Space Flight Center, Greenbelt, Maryland, 69 pp.

Jeffrey, S.W., R.F.C. Mantoura, and S.W. Wright (Eds.), 1997: *Phytoplankton Pigments in Oceanography: Guidelines to Modern Methods.* UNESCO Publishing, Paris, 661 pp.

Joint Global Ocean Flux Study, 1994: Protocols for the JGOFS core measurements, *UNESCO,* **29,** 91–96.

Kearns, E., R. Riley, and C. Woody, 1996: A bio-optical time series collected in coastal waters for SeaWiFS calibration and validation: Large structure shadowing considerations. Halifax, Canada, *Proc. SPIE,* Ocean Optics XIII, **2963,** 697–702.

Kirk, J.T.O., 1994: Estimation of the absorption and the scattering coefficients of natural waters by use of underwater irradiance measurements, *Appl. Opt.*, **33**, 3,276–3,278.

Kishino, M., J. Ishizaka, S. Saitoh, Y. Senga, and M. Utashima, 1997: Verification plan of ocean color and temperature scanner atmospheric correction and phytoplankton pigment by moored optical buoy system, *J. Geophys. Res.*, **102**, 17,197–17,207.

Maritorena, S., A. Morel, and B. Gentili, 1994: Diffuse reflectance of oceanic shallow water: influence of water depth and bottom albedo, *Limnol. Oceanogr.*, **39**, 1,689–1,703.

Mitchell, B.G., and D.A. Kiefer, 1988: Chlorophyll-*a* specific absorption and fluorescence excitation spectra for light-limited phytoplankton, *Deep-Sea Res.*, **35**, 639–663.

Morel, A., and Y.-H. Ahn, 1990: Optical efficiency factors of free-living marine bacteria: Influence of bacterioplankton upon the optical properties and particulate organic carbon in oceanic waters, *J. Mar. Res.*, **48**, 145–175.

Mueller, J.L., 1995: "Comparison of irradiance immersion coefficients for several marine environmental radiometers (MERs)." In: Case Studies for SeaWiFS Calibration and Validation. *NASA Tech. Memo. 104566, Vol. 27*, S.B. Hooker and E.R. Firestone, Eds., NASA Goddard Space Flight Center, Greenbelt, Maryland, 46 pp.

——, and R.W. Austin, 1995: Ocean Optics Protocols for SeaWiFS Validation, Revision 1. *NASA Tech. Memo. 104566, Vol. 25*, S.B. Hooker and E.R. Firestone, Eds., NASA Goddard Space Flight Center, Greenbelt, Maryland, 67 pp.

Pak, H., J.R.V. Zaneveld, and G.F. Beardsley, 1971: Mie scattering by suspended clay particles, *J. Geophys. Res.*, **76**, 5,065–5,069.

Pinkerton, M.H., and J. Aiken, 1999: Calibration and validation of remotely-sensed observations of ocean colour from a moored data buoy, *J. Atmos. Oceanic Technol.*, **16**, 915–923.

Pope, R.M., and E.S. Fry, 1997: Absorption spectrum (380–700 nm) of pure water. II. Integrating cavity measurements, *Appl. Opt.*, **36**, 8,710–8,723.

Press, W.H., S.A. Teukolsky, W.T. Vetterling, and B.P. Flannery, 1987: *Numerical Recipies in Fortran.* Cambridge University Press, 963 pp.

Shimada, M., H. Oaku, Y. Mitomi, H. Murakami, A. Mukaida, J. Ishizaka, H. Kawamura, T. Tanaka, M. Kishino, and H. Fukushima, 1998: Calibration and validation of Ocean Color Version-3 Product from ADEOS OCTS, *J. Oceanogr.*, **54**, 401–416.

Smirnov, A., B.N. Holben, O. Dubovik, N.T. O'Neill, L.A. Remer, T.F. Eck, I. Slustsker, and D. Savoie, 2000: Measurement of atmospheric optical parameters on U.S. Atlantic coast sites, ships and Bermuda during TARFOX, *J. Geophys. Res.*, **105**, 9,887–9,901.

Stramsky, D., and D.A. Kiefer, 1991: Light scattering by microorganisms in the open ocean, *Prog. Oceanogr.*, **28**, 343–383.

——, and C.D. Mobley, 1997: Effects of microbial particles on ocean optics: A database of single-particle optical properties, *Limnol. Oceanogr.*, **42**, 538–549.

Strickland, J.D.H., and T.R. Parsons, 1972: A practical handbook of sea water analysis. *Fish. Res. Board. Canada*, 310 pp.

Sturm, B., and G. Zibordi, 2002: SeaWiFS atmospheric correction by an approximate model and vicarious calibration, *Int. J. Remote Sens.*, **23**, 489–501.

Tassan, S., and G.M. Ferrari, 1995: An alternative approach to absorption measurements of aquatic particles retained on filters, *Limnol. Oceanogr.*, **40**, 1,358–1,368.

——, and ——, 2002: Sensitivity analysis of the "Transmittance-Reflectance" method for measuring light absorption by aquatic particles retained on filters, *J. Plankton Res.*, (submitted).

Twardowski, M.S., J.M. Sullivan, P.L. Donaghay, and J.R. Zaneveld, 1999: Microscale quantification of the absorption by dissolved and particulate material in coastal waters with AC-9, *J. Atmos. Oceanic Technol.*, **16**, 691–707.

Vidussi, V., H. Claustre, J. Bustillos-Guzmán, and J.C. Marty, 1996: Determination of chlorophylls and carotenoids of marine plankton: separation of chlorophyll *a* from divinyl-chlorophyll *a* and zeaxanthin from lutein, *J. Plankton Res.*, **18**, 2,377–2,382.

World Meteorological Organization, 1983: *Guide to the Meteorological Instruments and Methods of Observation*, WMO-N.8, 517 pp.

Zaneveld, J.R., J.C. Kitchen, and C. Moore, 1994: The scattering error coefficient of reflective absorption measurements, *Proc. SPIE, Ocean Optics XII*, **2,258**, 44–54.

Zibordi, G., and G.M. Ferrari, 1995: Instrument self-shading in underwater optical measurements: experimental data, *Appl. Opt.*, **34**, 2,750–2,754.

——, V. Barale, G.M. Ferrari, N. Hoepffner, L. Alberotanza, P. Cova, and C. Ramasco, 1995: Coastal Atmosphere and Sea Time-Series project (CoASTS): An ocean colour remote sensing calibration-validation project. *Proc. Third Thematic Conf. Remote Sens. Mar. Coastal Environ.*, Seattle, September 18–20, **2**, 96–100.

——, G.P. Doyle, and S. Hooker, 1999: Offshore tower-shading effects on in-water optical measurements, *J. Atmos. Oceanic Technol.*, **16**, 1,767–1,779.

——, and J-F. Berthon, 2001: *In situ* relationships between *Q*-factor and seawater optical properties in a coastal region, *Limnol. Oceanogr.*, **46**, 1,130–1,140.

——, S.B. Hooker, J-F. Berthon, and D. D'Alimonte, 2002: Autonomous above-water radiance measurements from an offshore platform: A field assessment experiment. *J. Atmos. Oceanic Technol.*, **19**, 808–819.

THE SeaWiFS POSTLAUNCH
TECHNICAL REPORT SERIES

Vol. 1

Johnson, B.C., J.B. Fowler, and C.L. Cromer, 1998: The Sea-WiFS Transfer Radiometer (SXR). *NASA Tech. Memo. 1998–206892, Vol. 1,* S.B. Hooker and E.R. Firestone, Eds., NASA Goddard Space Flight Center, Greenbelt, Maryland, 58 pp.

Vol. 2

Aiken, J., D.G. Cummings, S.W. Gibb, N.W. Rees, R. Woodd-Walker, E.M.S. Woodward, J. Woolfenden, S.B. Hooker, J-F. Berthon, C.D. Dempsey, D.J. Suggett, P. Wood, C. Donlon, N. González-Benítez, I. Huskin, M. Quevedo, R. Barciela-Fernandez, C. de Vargas, and C. McKee, 1998: AMT-5 Cruise Report. *NASA Tech. Memo. 1998–206892, Vol. 2,* S.B. Hooker and E.R. Firestone, Eds., NASA Goddard Space Flight Center, Greenbelt, Maryland, 113 pp.

Vol. 3

Hooker, S.B., G. Zibordi, G. Lazin, and S. McLean, 1999: The SeaBOARR-98 Field Campaign. *NASA Tech. Memo. 1999–206892, Vol. 3,* S.B. Hooker and E.R. Firestone, Eds., NASA Goddard Space Flight Center, Greenbelt, Maryland, 40 pp.

Vol. 4

Johnson, B.C., E.A. Early, R.E. Eplee, Jr., R.A. Barnes, and R.T. Caffrey, 1999: The 1997 Prelaunch Radiometric Calibration of SeaWiFS. *NASA Tech. Memo. 1999–206892, Vol. 4,* S.B. Hooker and E.R. Firestone, Eds., NASA Goddard Space Flight Center, Greenbelt, Maryland, 51 pp.

Vol. 5

Barnes, R.A., R.E. Eplee, Jr., S.F. Biggar, K.J. Thome, E.F. Zalewski, P.N. Slater, and A.W. Holmes 1999: The Sea-WiFS Solar Radiation-Based Calibration and the Transfer-to-Orbit Experiment. *NASA Tech. Memo. 1999–206892, Vol. 5,* S.B. Hooker and E.R. Firestone, Eds., NASA Goddard Space Flight Center, 28 pp.

Vol. 6

Firestone, E.R., and S.B. Hooker, 2000: SeaWiFS Postlaunch Technical Report Series Cumulative Index: Volumes 1–5. *NASA Tech. Memo. 2000–206892, Vol. 6,* S.B. Hooker and E.R. Firestone, Eds., NASA Goddard Space Flight Center, Greenbelt, Maryland, 14 pp.

Vol. 7

Johnson, B.C., H.W. Yoon, S.S. Bruce, P-S. Shaw, A. Thompson, S.B. Hooker, R.E. Eplee, Jr., R.A. Barnes, S. Maritorena, and J.L. Mueller, 1999: The Fifth SeaWiFS Intercalibration Round-Robin Experiment (SIRREX-5), July 1996. *NASA Tech. Memo. 1999–206892, Vol. 7,* S.B. Hooker and E.R. Firestone, Eds., NASA Goddard Space Flight Center, 75 pp.

Vol. 8

Hooker, S.B., and G. Lazin, 2000: The SeaBOARR-99 Field Campaign. *NASA Tech. Memo. 2000–206892, Vol. 8,* S.B. Hooker and E.R. Firestone, Eds., NASA Goddard Space Flight Center, 46 pp.

Vol. 9

McClain, C.R., E.J. Ainsworth, R.A. Barnes, R.E. Eplee, Jr., F.S. Patt, W.D. Robinson, M. Wang, and S.W. Bailey, 2000: SeaWiFS Postlaunch Calibration and Validation Analyses, Part 1. *NASA Tech. Memo. 2000–206892, Vol. 9,* S.B. Hooker and E.R. Firestone, Eds., NASA Goddard Space Flight Center, 82 pp.

Vol. 10

McClain, C.R., R.A. Barnes, R.E. Eplee, Jr., B.A. Franz, N.C. Hsu, F.S. Patt, C.M. Pietras, W.D. Robinson, B.D. Schieber, G.M. Schmidt, M. Wang, S.W. Bailey, and P.J. Werdell, 2000: SeaWiFS Postlaunch Calibration and Validation Analyses, Part 2. *NASA Tech. Memo. 2000–206892, Vol. 10,* S.B. Hooker and E.R. Firestone, Eds., NASA Goddard Space Flight Center, 57 pp.

Vol. 11

O'Reilly, J.E., S. Maritorena, M.C. O'Brien, D.A. Siegel, D. Toole, D. Menzies, R.C. Smith, J.L. Mueller, B.G. Mitchell, M. Kahru, F.P. Chavez, P. Strutton, G.F. Cota, S.B. Hooker, C.R. McClain, K.L. Carder, F. Müller-Karger, L. Harding, A. Magnuson, D. Phinney, G.F. Moore, J. Aiken, K.R. Arrigo, R. Letelier, and M. Culver 2000: SeaWiFS Postlaunch Calibration and Validation Analyses, Part 3. *NASA Tech. Memo. 2000–206892, Vol. 11,* S.B. Hooker and E.R. Firestone, Eds., NASA Goddard Space Flight Center, 49 pp.

Vol. 12

Firestone, E.R., and S.B. Hooker, 2000: SeaWiFS Postlaunch Technical Report Series Cumulative Index: Volumes 1–11. *NASA Tech. Memo. 2000–206892, Vol. 12,* S.B. Hooker and E.R. Firestone, Eds., NASA Goddard Space Flight Center, Greenbelt, Maryland, 24 pp.

Vol. 13

Hooker, S.B., G. Zibordi, J-F. Berthon, S.W. Bailey, and C.M. Pietras, 2000: The SeaWiFS Photometer Revision for Incident Surface Measurement (SeaPRISM) Field Commissioning. *NASA Tech. Memo. 2000–206892, Vol. 13,* S.B. Hooker and E.R. Firestone, Eds., NASA Goddard Space Flight Center, Greenbelt, Maryland, 24 pp.

Vol. 14

Hooker, S.B., H. Claustre, J. Ras, L. Van Heukelem, J-F. Berthon, C. Targa, D. van der Linde, R. Barlow, and H. Sessions, 2000: The First SeaWiFS HPLC Analysis Round-Robin Experiment (SeaHARRE-1). *NASA Tech. Memo. 2000–206892, Vol. 14,* S.B. Hooker and E.R. Firestone, Eds., NASA Goddard Space Flight Center, Greenbelt, Maryland, 42 pp.

Vol. 15

Hooker, S.B., G. Zibordi, J-F. Berthon, D. D'Alimonte, S. Maritorena, S. McLean, and J. Sildam, 2001: Results of the Second SeaWiFS Data Analysis Round Robin, March 2000 (DARR-00). *NASA Tech. Memo. 2001–206892, Vol. 15,* S.B. Hooker and E.R. Firestone, Eds., NASA Goddard Space Flight Center, Greenbelt, Maryland, 71 pp.

G. Zibordi, J.-F. Berthon, J.P. Doyle, S. Grossi, D. van der Linde, C. Targa, and L. Alberotanza

Vol. 16

Patt, F.S., 2002: Navigation Algorithms for the SeaWiFS Mission. *NASA Tech. Memo. 2002-206892, Vol. 16*, S.B. Hooker and E.R. Firestone, Eds., NASA Goddard Space Flight Center, Greenbelt, Maryland, 17 pp.

Vol. 17

Hooker, S.B., S. McLean, J. Sherman, M. Small, G. Lazin, G. Zibordi, and J.W. Brown, 2002: The Seventh SeaWiFS Intercalibration Round-Robin Experiment (SIRREX-7), March 1999. *NASA Tech. Memo. 2002-206892, Vol. 17*, S.B. Hooker and E.R. Firestone, Eds., NASA Goddard Space Flight Center, Greenbelt, Maryland, 69 pp.

Vol. 18

Firestone, E.R., and S.B. Hooker, 2002: SeaWiFS Postlaunch Technical Report Series Cumulative Index: Volumes 1–17. *NASA Tech. Memo. 2002-206892, Vol. 18*, S.B. Hooker and E.R. Firestone, Eds., NASA Goddard Space Flight Center, Greenbelt, Maryland, (in preparation).

Vol. 19

Zibordi, G., J.-F. Berthon, J.P. Doyle, S. Grossi, D. van der Linde, C. Targa, and L. Alberotanza 2002: Coastal Atmosphere and Sea Time Series (CoASTS), Part 1: A Tower-Based Long-Term Measurement Program. *NASA Tech. Memo. 2002-206892, Vol. 19*, S.B. Hooker and E.R. Firestone, Eds., NASA Goddard Space Flight Center, Greenbelt, Maryland, 29 pp.

REPORT DOCUMENTATION PAGE

1. AGENCY USE ONLY *(Leave blank)*	2. REPORT DATE June 2002	3. REPORT TYPE AND DATES COVERED Technical Memorandum

4. TITLE AND SUBTITLE

SeaWiFS Postlaunch Technical Report Series

Volume 19: Coastal Atmosphere and Sea Time Series (CoASTS), Part 1: A Tower-Based, Long-Term Measurement Program

5. FUNDING NUMBERS

970.2

6. AUTHORS

Giuseppe Zibordi, Jean-Françoise Berthon, John P. Doyle, Stefania Grossi, Dirk van der Linde, Cristina Targa, and Luigi Alberotanza

Series Editors: Stanford B. Hooker and Elaine R. Firestone

7. PERFORMING ORGANIZATION NAME(S) AND ADDRESS(ES)

Laboratory for Hydrospheric Processes
Goddard Space Flight Center
Greenbelt, Maryland 20771

8. PERFORMING ORGANIZATION REPORT NUMBER

2002-02645-0

9. SPONSORING/MONITORING AGENCY NAME(S) AND ADDRESS(ES)

National Aeronautics and Space Administration
Washington, D.C. 20546–0001

10. SPONSORING/MONITORING AGENCY REPORT NUMBER

TM—2002–206892, Vol. 19

11. SUPPLEMENTARY NOTES

E.R. Firestone: Science Applications International Corporation, Beltsville, Maryland; G. Zibordi, J-F. Berthon, J.P. Doyle, S. Grossi, D. van der Linde, and C. Targa: JRC/SAI/Marine Environment Unit, Ispra, Italy; and L. Alberotanza: CNR Institute for the Study of Dynamics of Large Masses, Venice, Italy

12a. DISTRIBUTION/AVAILABILITY STATEMENT

Unclassified–Unlimited
Subject Category 48
Report is available from the Center for AeroSpace Information (CASI),
7121 Standard Drive, Hanover, MD 21076–1320; (301)621-0390

12b. DISTRIBUTION CODE

13. ABSTRACT *(Maximum 200 words)*

The Coastal Atmosphere and Sea Time Series (CoASTS) Project, aimed at supporting ocean color research and applications, from 1995 up to the time of publication of this document, has ensured the collection of a comprehensive atmospheric and marine data set from an oceanographic tower located in the northern Adriatic Sea. The instruments and the measurement methodologies used to gather quantities relevant for bio-optical modeling and for the calibration and validation of ocean color sensors, are described. Particular emphasis is placed on four items: 1) the evaluation of perturbation effects in radiometric data (i.e., tower-shading, instrument self-shading, and bottom effects); 2) the intercomparison of seawater absorption coefficients from *in situ* measurements and from laboratory spectrometric analysis on discrete samples; 3) the intercomparison of two filter techniques for *in vivo* measurement of particulate absorption coefficients; and 4) the analysis of repeatability and reproducibility of the most relevant laboratory measurements carried out on seawater samples (i.e., particulate and yellow substance absorption coefficients, and pigment and total suspended matter concentrations). Sample data are also presented and discussed to illustrate the typical features characterizing the CoASTS measurement site in view of supporting the suitability of the CoASTS data set for bio-optical modeling and ocean color calibration and validation.

14. SUBJECT TERMS

SeaWiFS, Oceanography, CoASTS, Coastal Atmosphere Sea Time Series, AAOT, Pigment, Chlorophyll

15. NUMBER OF PAGES
29

16. PRICE CODE

17. SECURITY CLASSIFICATION OF REPORT	18. SECURITY CLASSIFICATION OF THIS PAGE	19. SECURITY CLASSIFICATION OF ABSTRACT	20. LIMITATION OF ABSTRACT
Unclassified	Unclassified	Unclassified	Unlimited